Jets and Radio Loud AGN

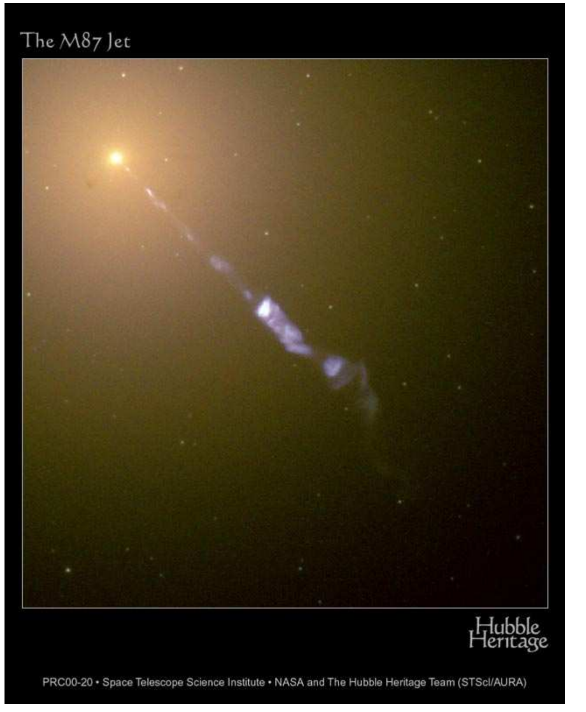

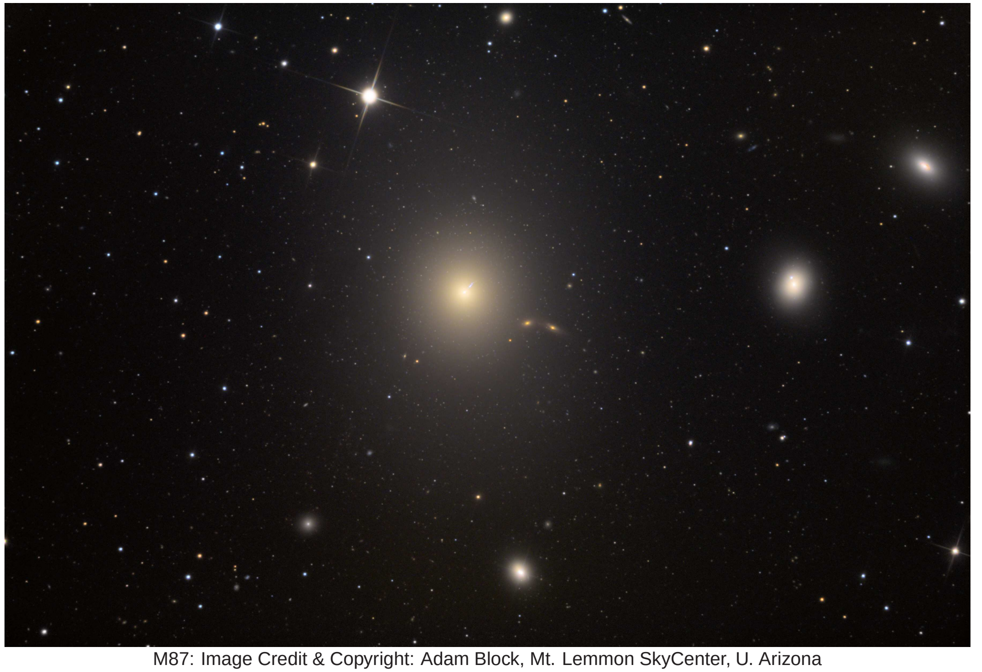

M87: Image Credit & Copyright: Adam Block, Mt. Lemmon SkyCenter, U. Arizona

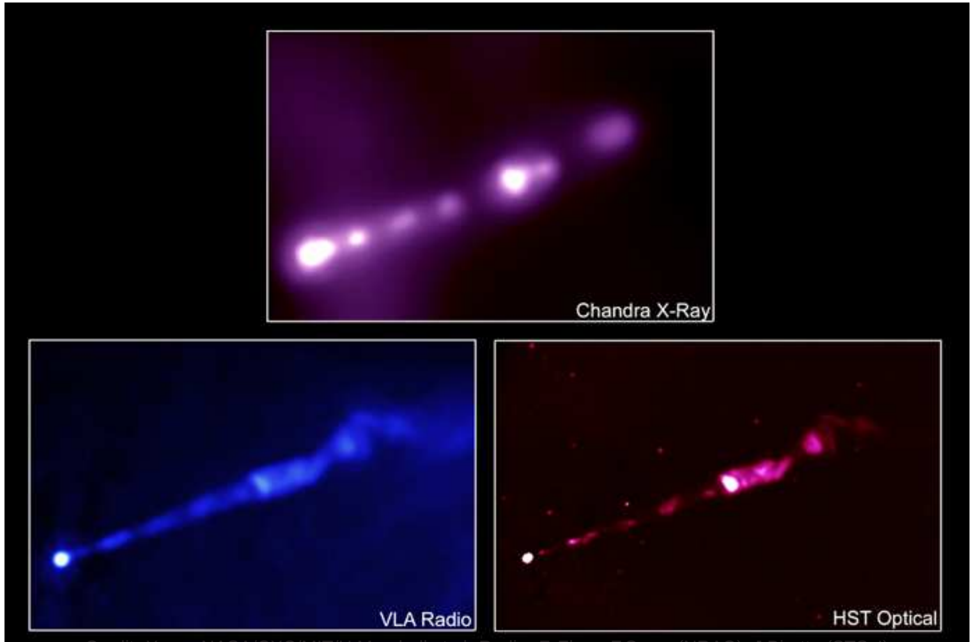

Credit: X-ray: NASA/CXC/MIT/H.Marshall et al. Radio: F. Zhou, F.Owen (NRAO), J.Biretta (STScI)

Optical: NASA/STScI/UMBC/E.Perlman et al.

AGN Jets

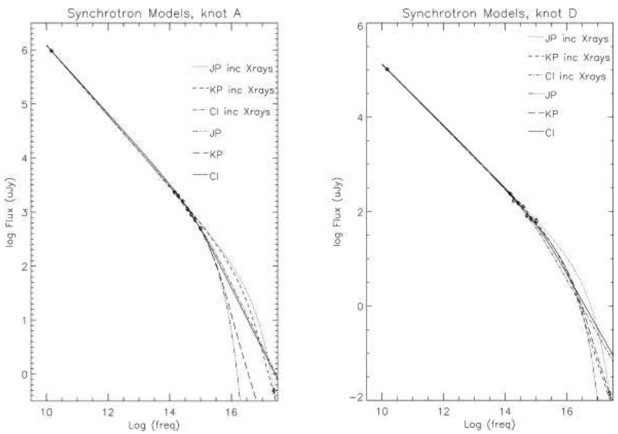

(M87; Perlman et al., 2002)

Spectral shape of jet emission is a power law $\Longrightarrow$ synchrotron radiation

Typical power law index: $\alpha \sim 0.65$ between radio and optical.

Outline

Jets are broadband emitters! First consider the radio band. Then move on to higher energies.

Most important jet emission process in the radio band: synchrotron radiation.

Synchrotron-Radiation (=Magnetobremsstrahlung): Radiation emitted by relativistic electrons in a magnetic field.

Outline for the following discussion of theory of synchrotron-radiation: Short and qualitative description. See Rybicki & Lightman (1979, Chapters 3, 6, and 7).

1. Motion of electrons in magnetic fields,
2. Look at emission from a single electron,
3. Consider electron distribution and opacity effects to obtain the final spectrum.
4. Consider processes to transfer the primary synchrotron emission to the highest energies (if needed).

Relativistic Motion

Moving electron in magnetic field ($\boldsymbol{E} = 0$): In Gaussian units, the Lorentz-Force is

$$\frac{d\boldsymbol{p}}{dt} = \frac{e}{c}\boldsymbol{v} \times \boldsymbol{B} \quad \text{where} \quad \boldsymbol{p} = \frac{m_\mathrm{e}\boldsymbol{v}}{\sqrt{1-\beta^2}} = \gamma m_\mathrm{e}\boldsymbol{v} \tag{10.1}$$

where

$$\gamma = \frac{1}{\sqrt{1-\beta^2}} \quad \text{and where} \quad \beta = \frac{v}{c} \tag{10.2}$$

Therefore the acceleration is

$$\frac{d\boldsymbol{v}}{dt} = \frac{e}{c\gamma m_\mathrm{e}}\boldsymbol{v} \times \boldsymbol{B} \tag{10.3}$$

Since $\boldsymbol{v} \times \boldsymbol{B}$ is always perpendicular to $\boldsymbol{v}$ and $\boldsymbol{B}$, the component of $\boldsymbol{v}$ along the B-field does not change. This constant perpendicular force results to a helical motion around the B-field line with the frequency

$$\omega_B = \frac{eB}{\gamma m_\mathrm{e} c} = \frac{\omega_\mathrm{L}}{\gamma} \tag{10.4}$$

where the Larmor frequency (also Cyclotron frequency, gyrofrequency)

$$\omega_\mathrm{L} = 2\pi\nu_\mathrm{L} = \frac{eB}{m_\mathrm{e}c} \tag{10.5}$$

Numerical values

Numerically, the Larmor frequency is

$$\nu_\mathrm{L} = 2.8 B_{1\,\mathrm{G}}\,\mathrm{MHz} \tag{10.6}$$

The radius of the orbit (Larmor radius) is

$$R_\mathrm{L} = \frac{\gamma v_\perp}{\omega_\mathrm{L}} \sim 2\,\mathrm{AU} \cdot \frac{E}{1\,\mathrm{GeV}} \cdot \left(\frac{B}{10^{-6}\,\mathrm{G}}\right)^{-1} \tag{10.7}$$

$$\sim 300\,\mathrm{km} \cdot \frac{E}{1\,\mathrm{GeV}} \cdot \left(\frac{B}{1\,\mathrm{G}}\right)^{-1} \tag{10.8}$$

i.e., small on cosmical scales

Units and orders of magnitude:

- $1\,\mathrm{G} = 10^{-4}\,\mathrm{T}$,
- the typical B-field in the interstellar medium is $\sim 10^{-6}\,\mathrm{G}$,
- close to the centers of AGN $B \sim 1\,\mathrm{G}$.

Radiated Energy, I

Motion around B-field lines: acceleration.

But accelerated charges emit radiation (Larmor's formula):

$$P = \frac{dW}{dt} = \frac{q^2 \dot{v}^2}{4\pi c^3} \int \sin^2\theta\,\mathrm{d}\Omega = \frac{2q^2\dot{v}^2}{3c^3} \tag{10.9}$$

Assumption of isotropic velocity distribution, relativistic electrons ($\beta \longrightarrow 1$), and a messy derivation (see Rybicki & Lightman) yields for the average emitted power of an electron in a B-field

$$\langle P_\mathrm{em} \rangle = \frac{4}{3}\beta^2\gamma^2 c \sigma_\mathrm{T} U_B \tag{10.10}$$

with $U_B = B^2/8\pi$, the magnetic field energy density, and $\sigma_\mathrm{T} = 8\pi e^2/(3m_\mathrm{e}^2c^4)$, the Thomson cross section.

Note: Since $E = \gamma m_\mathrm{e} c^2 \Longrightarrow P \propto E^2 U_\mathrm{B}$.

Note: $P_\mathrm{em} \propto \sigma_\mathrm{T} \propto m_\mathrm{e}^{-2} \Longrightarrow$ Synchrotron radiation from charged particles with larger mass (protons,...) is negligible.

Note: Life-time of particles of energy E is

$$t_{1/2} \sim \frac{E}{P} \propto \frac{1}{B^2 E} = 5\,\mathrm{s}\left(\frac{B}{1\,\mathrm{T}}\right)^{-2}\gamma^{-1} = 1.6\times10^7\,\mathrm{years}\left(\frac{B}{10^{-7}\,\mathrm{T}}\right)^{-2}\gamma^{-1} \tag{10.11}$$

Radiated Energy, II

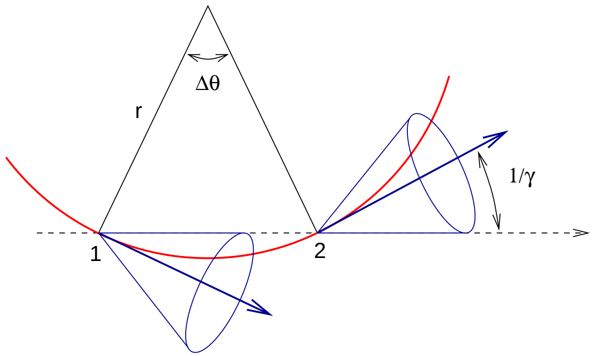

(after Fig. 6.2 of Rybicki & Lightman, 1979)

Relativistic electrons: radiation is forward beamed into cone with opening angle $\Delta\theta \sim 1/\gamma$. In the Electron frame of rest: beam passes observer during time

$$\Delta t = \frac{\Delta\theta}{\omega_B} = \frac{m_\mathrm{e} c\gamma}{eB}\frac{2}{\gamma} = \frac{2}{\omega_\mathrm{L}} \tag{10.12}$$

Radiated Energy, III

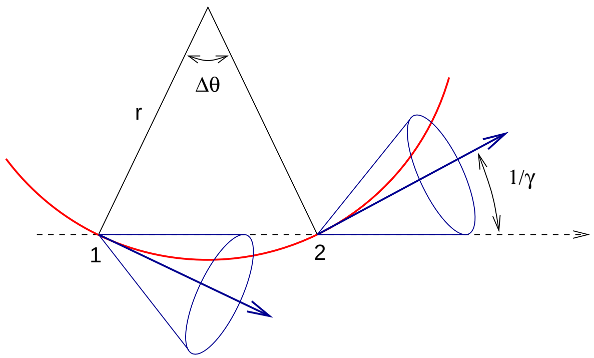

(after Fig. 6.2 of Rybicki & Lightman, 1979)

Observer frame: Doppler effect! (electron is closer to us at end of time interval)

$\Longrightarrow$ observed pulse duration:

$$\tau = \left(1 - \frac{v}{c}\right)\Delta t = (1-\beta)\Delta t \tag{10.13}$$

Radiated Energy, IV

For $\gamma \gg 1$, i.e., $\beta = v/c \sim 1$

$$\frac{1}{\gamma^2} = 1 - \frac{v^2}{c^2} = (1+\beta)(1-\beta) \approx 2(1-\beta) \tag{10.14}$$

such that

$$\tau = (1-\beta)\Delta t = \frac{1}{2}\left(1 - \frac{v^2}{c^2}\right)\Delta t = \frac{1}{\gamma^2 \omega_\mathrm{L}} \tag{10.15}$$

Thus the characteristic frequency of the radiation is given by

$$\omega_\mathrm{c} = \gamma^2 \omega_\mathrm{L} = \frac{eB}{m_\mathrm{e}c}\left(\frac{E}{m_\mathrm{e}c^2}\right)^2 \tag{10.16}$$

Short gyration pulses $\Longrightarrow$ broad spectrum (Heisenberg: $\Delta\omega\Delta t > 1$) with the highest frequency in the regime of $\nu_\mathrm{c} = \omega_\mathrm{c}/2\pi$.

Nonthermal Synchrotron Radiation, I

For an electron distribution, $n(\gamma)$, the emitted spectrum is found by properly weighting contributions of electrons with different energies:

$$P_\nu = \int_1^\infty P_\nu(\gamma) n(\gamma) d\gamma \tag{10.17}$$

Most important case: nonthermal synchrotron radiation, where electrons have a power-law distribution

$$n(\gamma)d\gamma = n_0 \gamma^{-p} d\gamma \quad . \tag{10.18}$$

The spectral energy distribution P_ν of an electron with total energy $E = \gamma m_\mathrm{e} c^2$ can be written as

$$P_\nu(\gamma) = \frac{4}{3}\beta^2\gamma^2 c\sigma_\mathrm{T} U_\mathrm{B} \phi_\nu(\gamma) \tag{10.19}$$

where the spectral shape is described by a function $\phi_\nu(\gamma)$ with

$$\int \phi_\nu(\gamma) \mathrm{d}\gamma = 1 \quad . \tag{10.20}$$

Nonthermal Synchrotron Radiation, II

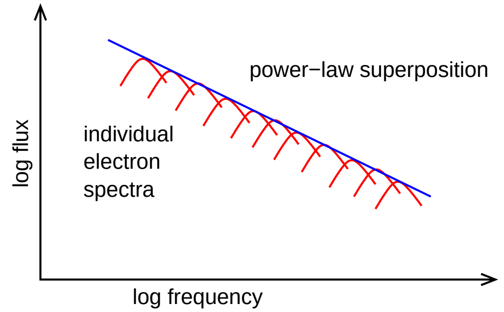

after (Shu, 1991, Fig. 18.4)

Assume that photons are only emitted at the characteristic frequency $\gamma^2\nu_\mathrm{L}$ (Eq. 10.16).

this is a good approximation since the spectrum emitted by an electron has a strong peak at that frequency

Therefore

$$\phi_\nu(\gamma) \sim \delta(\nu - \gamma^2\nu_\mathrm{L}) \tag{10.21}$$

Therefore the emitted power at frequency ν (=spectrum) is

$$P_\nu = \int_1^\infty \langle P_\nu(\gamma)\rangle \, n(\gamma) \mathrm{d}\gamma \tag{10.22}$$

Nonthermal Synchrotron Radiation, III

Therefore, for the electron power-law distribution Eq. 10.18

$$P_\nu = \int_1^\infty \frac{4}{3}\beta^2\gamma^2 c\sigma_\mathrm{T} U_\mathrm{B} \delta(\nu - \gamma^2\nu_\mathrm{L}) n_0 \gamma^{-p} \mathrm{d}\gamma \tag{10.23}$$

since $\gamma \gg 1$: $\beta \approx 1$

$$= A \int_1^\infty \gamma^{2-p} \delta(\nu - \gamma^2\nu_\mathrm{L}) \mathrm{d}\gamma \tag{10.24}$$

substituting $\nu' = \gamma^2\nu_\mathrm{L}$, i.e., $\mathrm{d}\nu' = \nu_\mathrm{L} 2\gamma \mathrm{d}\gamma$

$$= B \int_{\nu_\mathrm{L}}^\infty \gamma^{1-p} \delta(\nu - \nu') \mathrm{d}\nu' \tag{10.25}$$

since $\gamma = (\nu'/\nu_\mathrm{L})^{1/2}$, we find

$$P_\nu = \frac{2}{3} c\sigma_\mathrm{T} n_0 \frac{U_\mathrm{B}}{\nu_\mathrm{L}} \left(\frac{\nu}{\nu_\mathrm{L}}\right)^{-\frac{p-1}{2}} \tag{10.26}$$

The spectrum of an electron power-law distribution is a power-law!

Summary of Synchrotron Radiation Process

What we have done so far:

1. Motion of the electron
2. Radiation characteristic from relativistic motion
3. Doppler-effect
4. Integration over electron distribution

It is possible to do the same analytically without any approximations. This is too complicated to be done here. See the references for details.

Synchrotron Self-Absorption

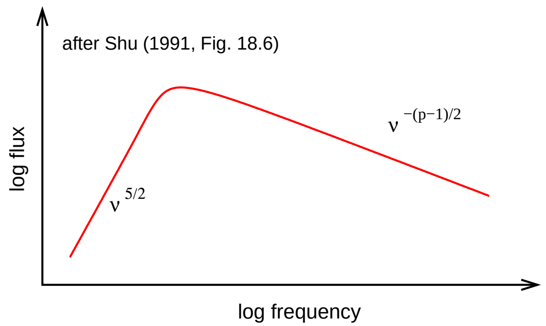

At low ν: synchrotron emitting electrons can absorb synchrotron photons:
synchrotron self-absorption.

For a power law electron distribution $\propto E^{-p}$, total spectral shape is:

For low frequencies: $P_\nu \propto B^{-1/2}\nu^{5/2}$ (independent of p!)
For large frequencies: $P_\nu \propto \nu^{-(p-1)/2}$

One often uses the terms optically thick/thin to describe the absorbed/unabsorbed part of a synchrotron spectrum. The turnover describes the $\tau = 1$ surface, e.g., of a jet. In general: $\tau \propto R$ (R: size of the emitting region). More compact regions are optically thick, more extended regions are optically thin.

Polarization of Synchrotron Radiation

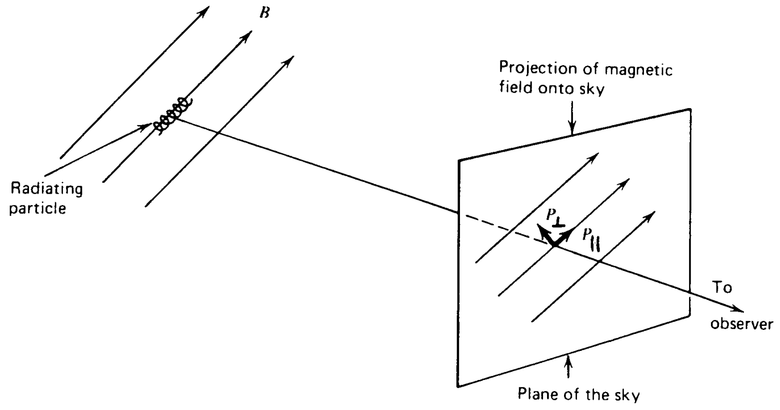

(Rybicki & Lightman, 1979, Fig. 6.7)

Exact calculation needs to take into account polarization of synchrotron radiation.

Polarization of Synchrotron Radiation

Result of exact calculation for both polarization directions:

$$\begin{pmatrix} P_\parallel \\ P_\perp \end{pmatrix} = \frac{\sqrt{3}e^3 B}{2\ mc^2} \begin{pmatrix} F(\nu/\nu_c) - G(\nu/\nu_c) \\ F(\nu/\nu_c) + G(\nu/\nu_c) \end{pmatrix} \tag{10.27}$$

where

$$F(x) = x\int_x^\infty K_{5/3}(y)\,dy \tag{10.28}$$

$$G(x) = xK_{2/3}(x) \tag{10.29}$$

and K_i are modified Bessel-functions of i-th order

Polarization allows to measure the magnetic field direction

$$F(x) = x\int_x^{\infty} K_{5/3}(\eta)d\eta \quad \text{and} \quad G(x) = xK_{2/3}(x)$$

x	$F(x)$	$G(x)$	x	$F(x)$	$G(x)$
0	0	0	0.90	0.694	0.521
0.001	0.213	0.107	1.0	0.655	0.494
0.005	0.358	0.184	1.2	0.566	0.439
0.01	0.445	0.231	1.4	0.486	0.386
0.025	0.583	0.312	1.6	0.414	0.336
0.050	0.702	0.388	1.8	0.354	0.290
0.075	0.772	0.438	2.0	0.301	0.250
0.10	0.818	0.475	2.5	0.200	0.168
0.15	0.874	0.527	3.0	0.130	0.111
0.20	0.904	0.560	3.5	0.0845	0.0726
0.25	0.917	0.582	4.0	0.0541	0.0470
0.29	0.918	0.592	4.5	0.0339	0.0298
0.30	0.918	0.596	5.0	0.0214	0.0192
0.40	0.901	0.607	6.0	0.0085	0.0077
0.50	0.872	0.603	7.0	0.0033	0.0031
0.60	0.832	0.590	8.0	0.0013	0.0012
0.70	0.788	0.570	9.0	0.00050	0.00047
0.80	0.742	0.547	10.0	0.00019	0.00018

Polarization of Synchrotron Radiation

The total emitted power for monoenergetic electrons is

$$P(\nu) = P_{\parallel}(\nu) + P_{\perp}(\nu) \propto F(\nu) \tag{10.30}$$

As before, the total emitted spectrum is found by integrating over the electron energy distribution. For a power-law:

$$\begin{pmatrix} P_{\parallel}(\nu) \\ P_{\perp}(\nu) \end{pmatrix} = \left(\frac{\sqrt{3}}{2}\right) n_0 \frac{e^3 B}{m_e c^2} \begin{pmatrix} J_F - J_G \\ J_F + J_G \end{pmatrix} \left(\frac{2\nu}{3\nu_L}\right)^{-(p-1)/2} \tag{10.31}$$

where

$$J_F = \frac{2^{(p+1)/2}}{p+1} \Gamma\left(\frac{p}{4} + \frac{19}{12}\right) \Gamma\left(\frac{p}{4} - \frac{19}{12}\right) \tag{10.32}$$

$$J_G = 2^{(p-3)/2} \Gamma\left(\frac{p}{4} + \frac{7}{12}\right) \Gamma\left(\frac{p}{4} - \frac{1}{12}\right) \tag{10.33}$$

$\Gamma(x) = \int_0^{\infty} t^{-x} e^{-t} dt$ is the Gamma-function.

Polarization of Synchrotron Radiation

The degree of polarization is defined by

$$\text{degree of polarization} := \frac{P_{\perp} - P_{\parallel}}{P_{\perp} + P_{\parallel}} \tag{10.34}$$

For a power law electron distribution:

$$\frac{P_{\perp} - P_{\parallel}}{P_{\perp} + P_{\parallel}} = \frac{J_G}{J_F} = \frac{p+1}{p+7/3} \tag{10.35}$$

For $p = 2.5$ the degree of polarization is $\sim 70\%$. This is very large!!

Caveat: Faraday-rotation and B-field inhomogeneities can decrease the degree of polarization.

Introduction, I

The powerful radio galaxy Cygnus A at $z = 0.057$ ($d = 230$ Mpc).

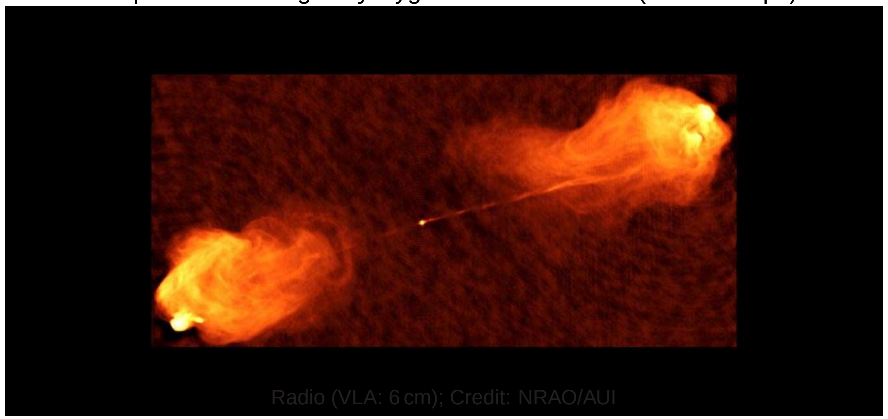

Size: $\sim$ 2.2 arcmin $\sim$ 600000 ly, about eight times the size of the milky way!

Radio morphology: Core – Jets – Hotspots – Lobes

Introduction, II

The powerful radio galaxy Cygnus A at $z = 0.057$ ($d = 230$ Mpc).

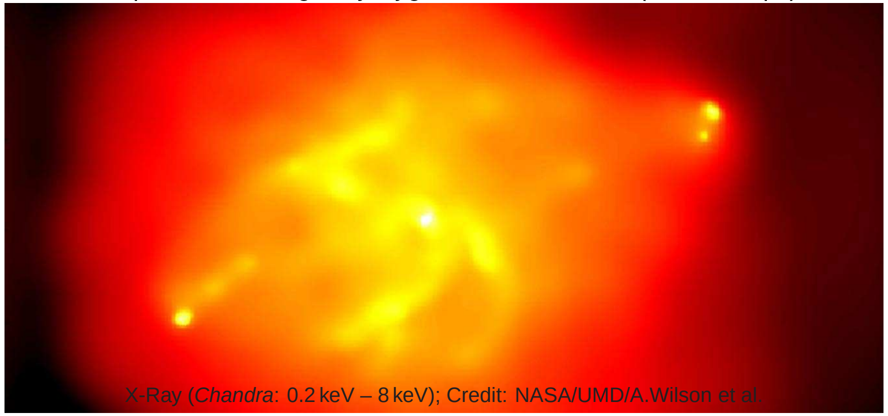

X-Ray (*Chandra*: 0.2 keV – 8 keV); Credit: NASA/UMD/A.Wilson et al.

Size: $\sim$ 2.2 arcmin $\sim$ 600000 ly, about eight times the size of the milky way!

Radio morphology: Core – Jets – Hotspots – Lobes

X-Ray morphology: Nucleus – Cavity – Hotspots

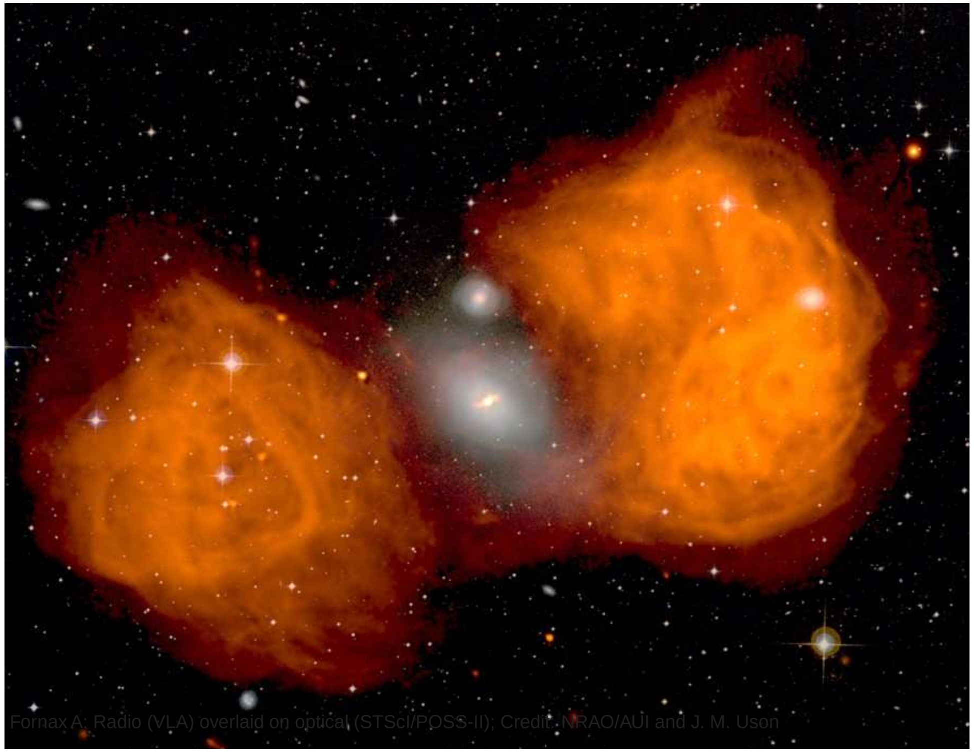

Fornax A: Radio (VLA) overlaid on optical (STScI/POSS-II); Credit: NRAO/AUI and J. M. Uson

Classification, I

At arcsec resolution, most radio-loud AGN are unresolved! But great variety in spectral shape.

Condon et al. (1998); Kuehr et al. (1981)

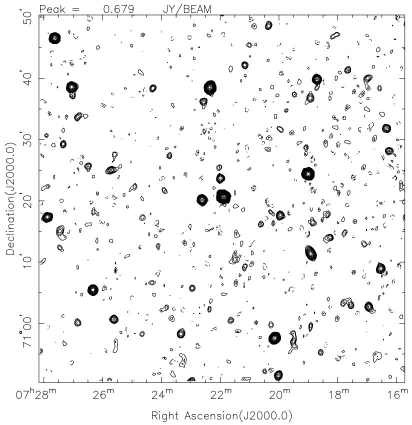

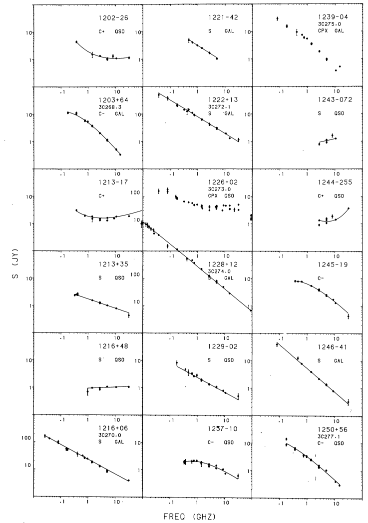

Classification, II

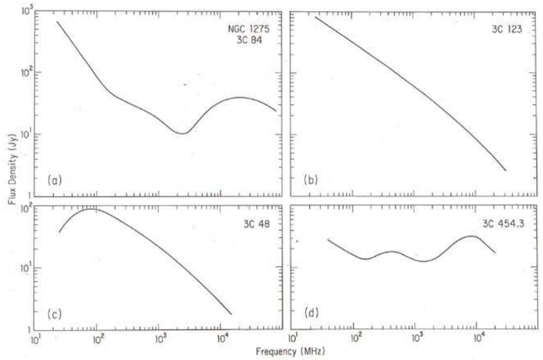

- NGC 1275: extended steep-spectrum emission plus compact self-absorbed nucleus
- 3C123: 3C 123: optically thin at all plotted frequencies
- 3C 48: self-absorbed below 100 MHz
- 3C454.3: superposition of many jet regions which become opaque at different frequencies (flat-spectrum radio quasar)

Classification, III

Classification based on morphology and radio spectrum:

1. Powerful double-lobed radio galaxies with hotspots and a steep radio spectrum falling toward higher frequencies (Fanaroff-Riley class II, FR II)
2. Weaker steep-spectrum, double-lobed radio galaxies without leading hotspots (FR I types)
3. Core-dominated flat-spectrum sources (Blazars: quasars and BL Lac objects)
4. Compact steep-spectrum sources (CSS sources) and gigahertz-peaked spectrum sources (GPS sources); no large-scale radio structure; morphological classification term: compact symmetric objects (CSOs) or compact doubles

Observing technique and frequency strongly affects sample composition (e.g., low-frequency flux-density limited surveys tend to select steep-spectrum sources. Flat-spectrum sources are classical targets for Very-Long-Baseline Interferometry (VLBI) observations, which are sensitive to compact emission.

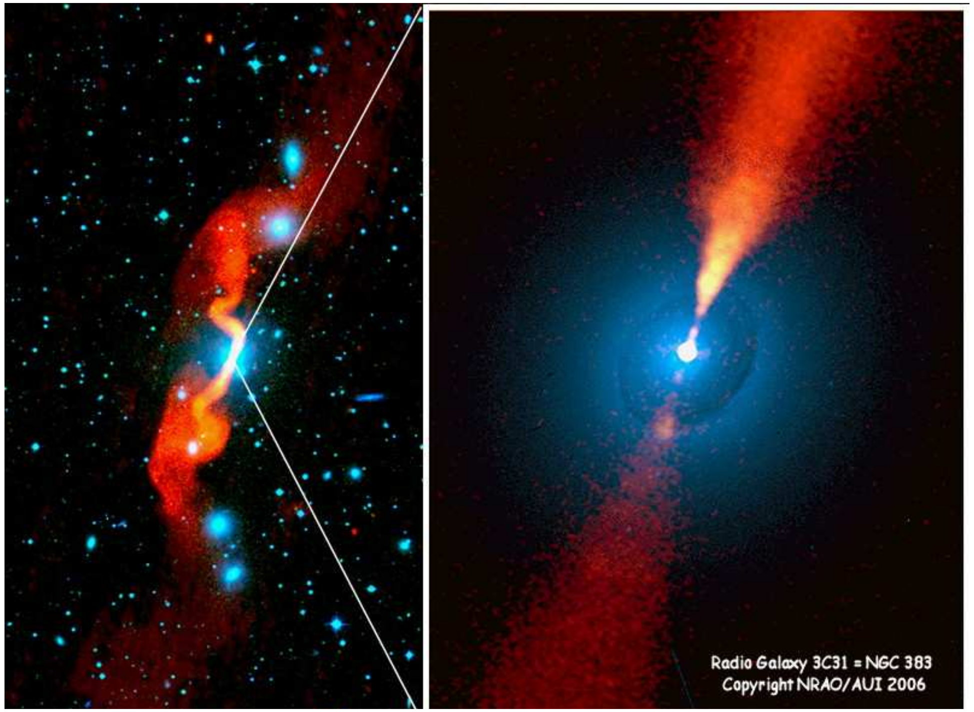

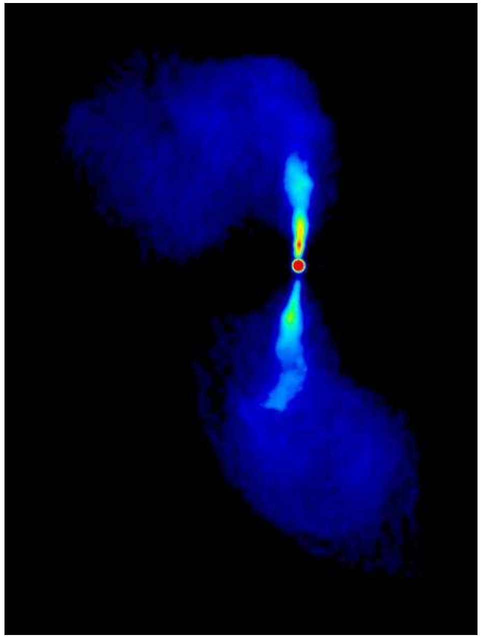

Fanaroff-Riley Type 1: asymmetric jets with wide opening angle ending in plumes

M84 (3C272.1) (Laing & Bridle, 1987):
VLA 4885 MHz, 134″ × 170″; see also
`www.jb.man.ac.uk/atlas/other/3C272P1.html`

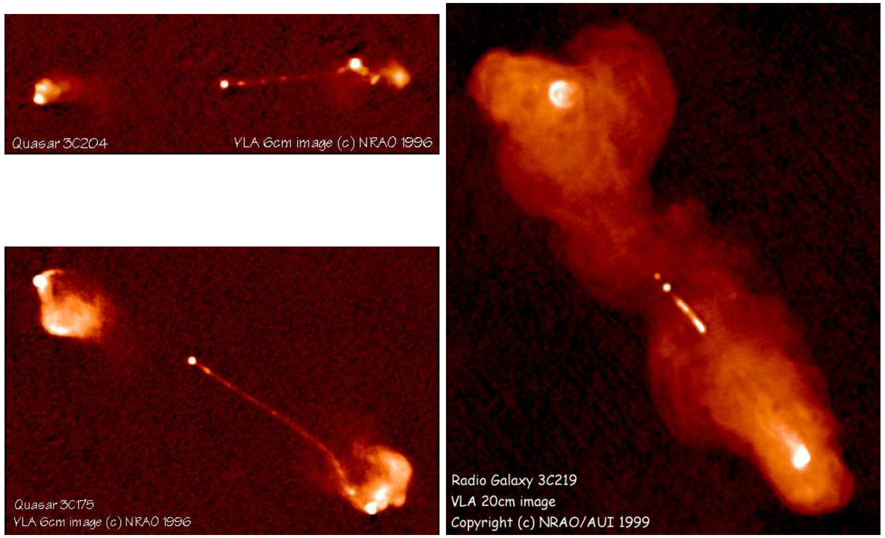

A. Bridle, `www.cv.nrao.edu/~abridle/images.htm`

Fanaroff-Riley Type 2: powerful lobe dominated doubles; jets often one-sided

Classification, VII

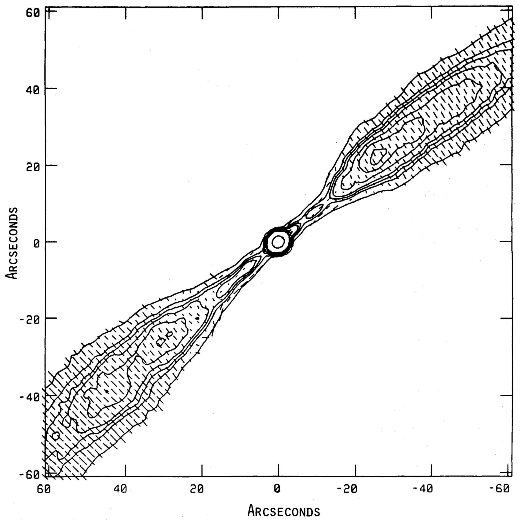

polarization in two-sided jet sources (FR 1): up to 40%
$\Rightarrow$ Synchrotron Radiation

B-field orientation:

- close to core: $B \parallel$ jet axis
- away from core ($\sim$10% jet length): $B \perp$ jet axis

B-field can change orientation again in knots

(B-field configuration in IC 4296; Killeen, Bicknell & Ekers, 1986, Fig. 25b)

Radio Interferometry: Longer baselines and higher frequencies yield higher resolution

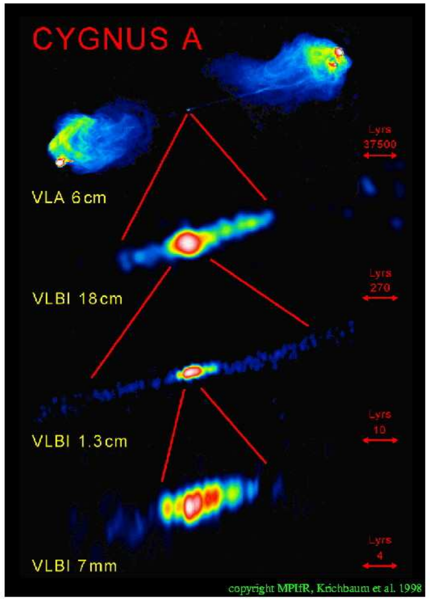

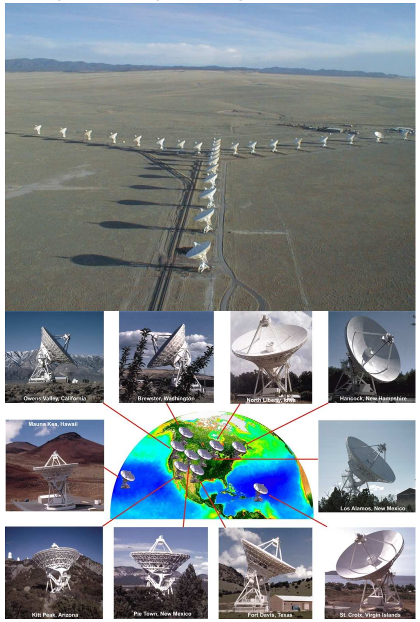

Image courtesy of MPIfR, NRAO/AUI and Earth image courtesy of the SeaWiFS Project NASA/GSFC and ORBIMAGE

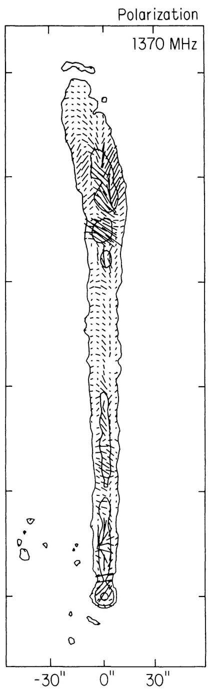

polarization in one-sided jet sources (FR 2): similar to FR 1, i.e., 40% and higher

B-field orientation in FR 2: parallel to jet axis throughout the jet

(E-field configuration in NGC 6251, note: B-field is perpendicular to E-field!; Perley, Bridle & Willis, 1984, Fig. 17)

Multifrequency VLBI Observations, I

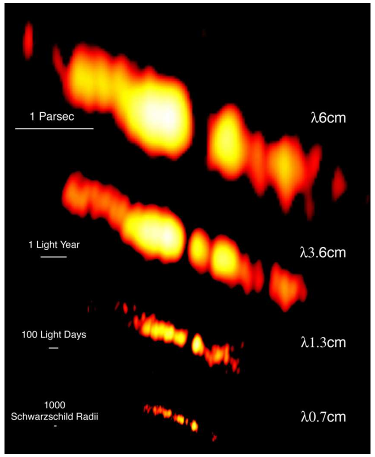

The Twin-Jet in NGC 1052 observed with the VLBA at 4 frequencies; Image: M. Kadler

At higher frequencies

1. the angular resolution improves
2. the structure changes: different parts of the jet dominate the emission at different frequencies (superposition to a flat spectrum)
3. emission shows up in the central emission gap; spectral index $\alpha > 2.5 \Rightarrow$ no self absorption
4. the absorption is caused by free-free absorption in the circumnuclear torus; at high frequencies, the torus becomes transparent

Kameno et al. (2001); Kadler et al. (2004)

Multifrequency VLBI Observations, II

Movie: Spinning the dial on NGC 1052

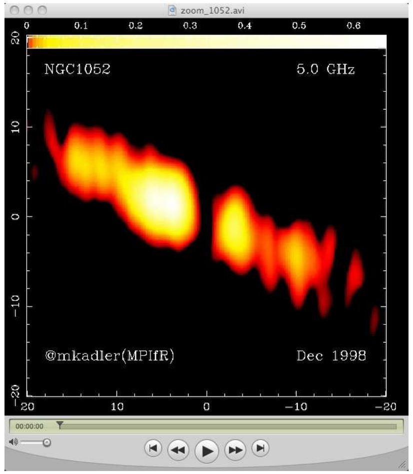

http://www.sternwarte.uni-erlangen.de/~kadler/movies/zoom_1052.avi

Flat-Spectrum Radio Sources: Blazars

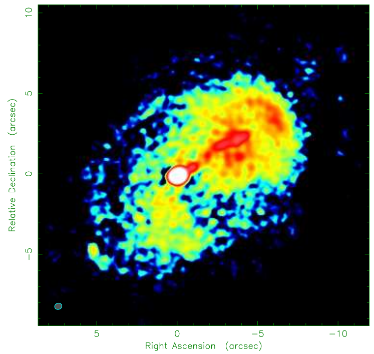

Image courtesy: U. Bach, MPIfR

0716+714, BL Lac object at redshift $z = 0.3$ (Nilsson et al., 2008)

Highly variable, core dominated object

"Fried-egg" morphology – really the end-on view of a radio lobe?

Almost all the flux density is concentrated within a few milliarcseconds-size compact jet!

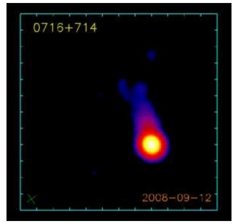

Image Courtesy: MOJAVE

"Roughly equal numbers of steep-spectrum extended double-lobed sources and flat-spectrum objects that are unresolved on arcsec scales." (Zensus, 1997)

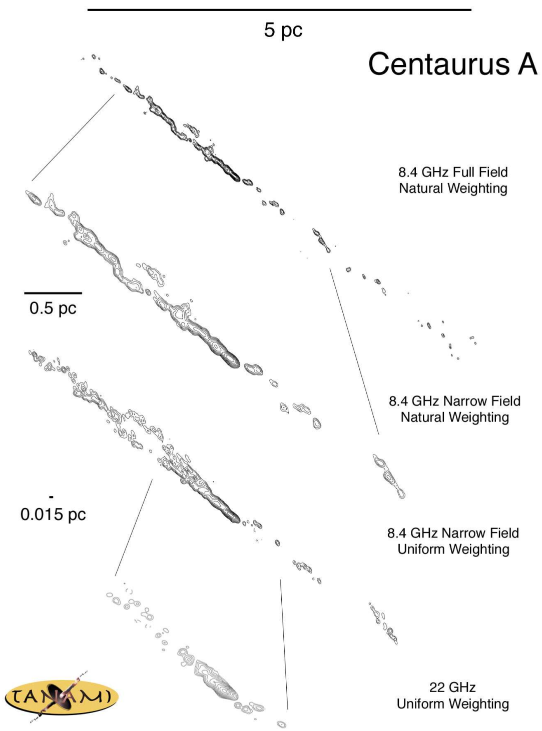

Superluminal Motion, I

VLBI resolution 1 mas

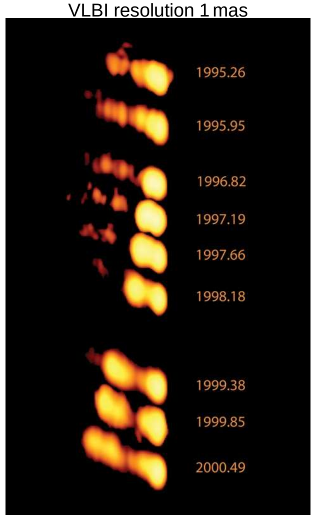

Kadler et al. (2008)

3C 111: Apparent speed of jet: $\sim 5c$

Superluminal motion: The apparent velocities of jet features ("blobs") measured in many AGN jets often exceed the speed of light.

First discovered in 1971 in 3C279 (Cohen et al., 1971; Whitney et al., 1971).

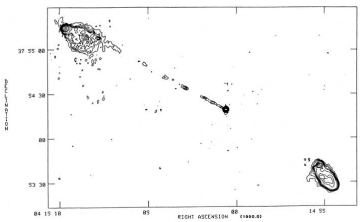

VLA resolution $\sim$ 1 arcsec

Superluminal Motion, II

Movies: Examples of superluminal motion in AGN jets

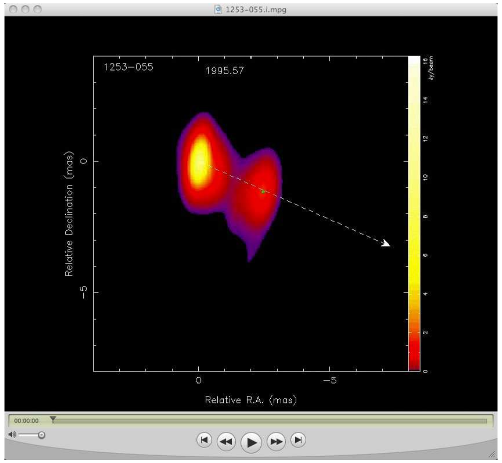

http://www.physics.purdue.edu/astro/MOJAVE/movies.html

Superluminal Motion Demo:

www.physics.purdue.edu/MOJAVE/superluminal.swf

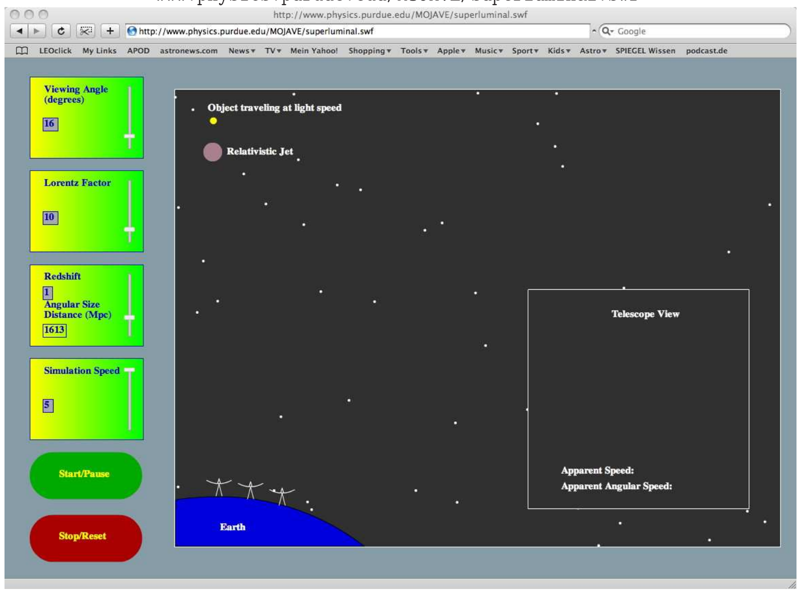

$t_1 = 0$: Blob is ejected from core and emits first photon.

Superluminal Motion Demo:

www.physics.purdue.edu/MOJAVE/superluminal.swf

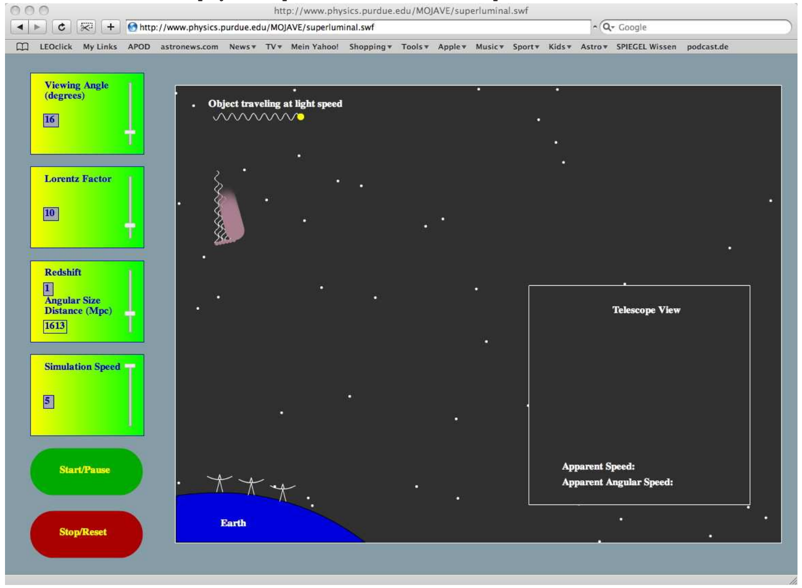

t_2: First photons and blob travel towards earth.

Superluminal Motion Demo:

www.physics.purdue.edu/MOJAVE/superluminal.swf

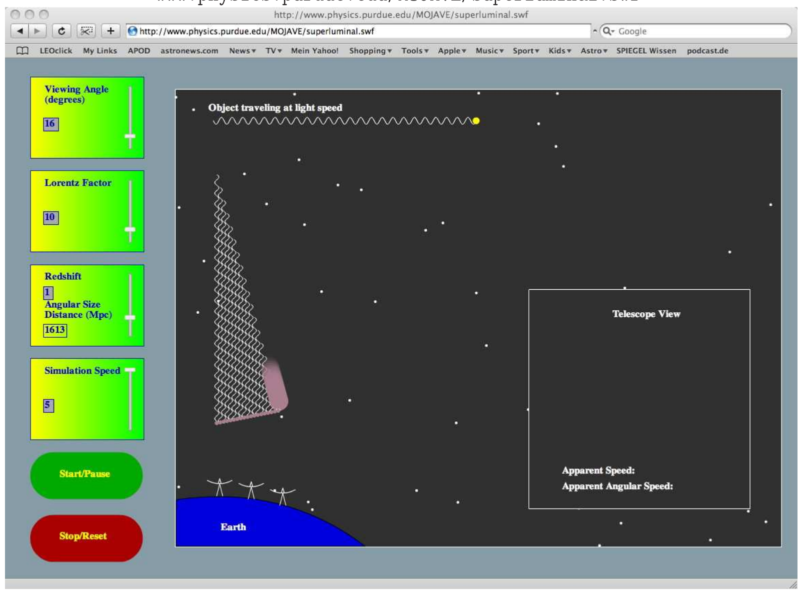

t_3: Blob almost keeps the pace of the photons.

Superluminal Motion Demo:

`www.physics.purdue.edu/MOJAVE/superluminal.swf`

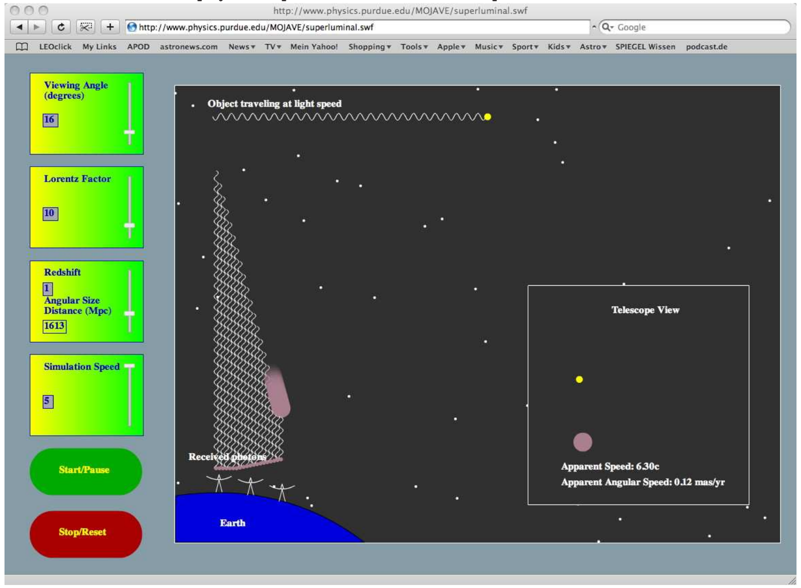

t_4: First photons arrive at telescope. Observer starts to take the time.

Superluminal Motion Demo:

`www.physics.purdue.edu/MOJAVE/superluminal.swf`

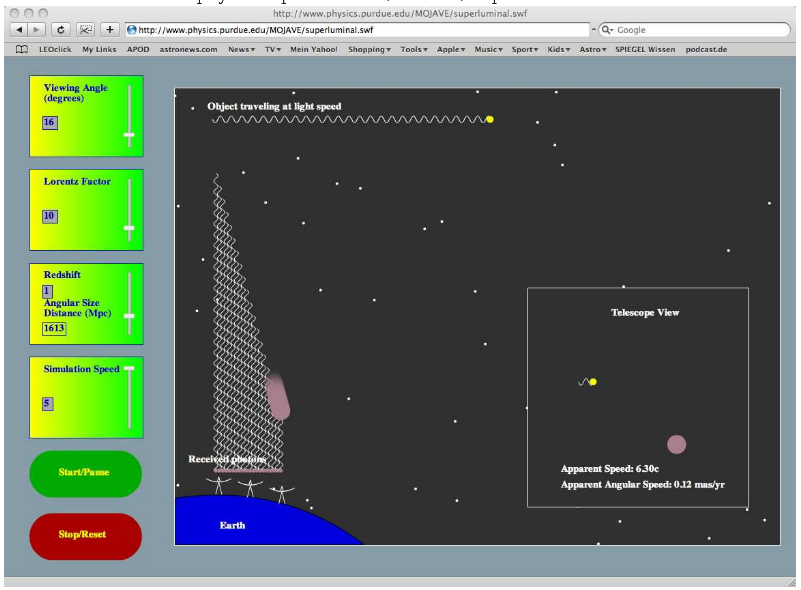

t_5: The last photons have a much smaller way to travel and come in quickly. Observer measures superluminal motion on the sky!

Superluminal Motion, VIII

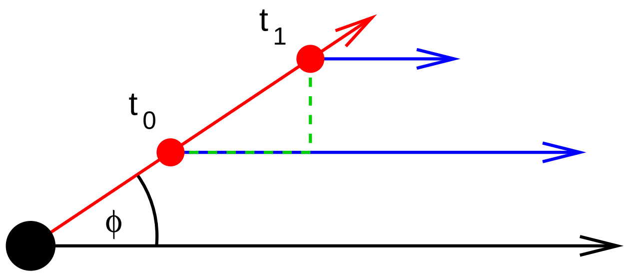

Consider blob moving towards us with speed v and angle ϕ with respect to line of sight, emitting light signals at t_0 and $t_1 = t_0 + \Delta t_\mathrm{e}$

Light travel time: Observer sees signals separated by

$$\Delta t_\mathrm{o} = \Delta t_\mathrm{e} - \Delta t_\mathrm{e}\frac{v}{c}\cos\phi = \left(1 - \frac{v}{c}\cos\phi\right)\Delta t_\mathrm{e} \tag{10.36}$$

Observed distance traveled in plane of sky:

$$\Delta\ell_\perp = v\Delta t_\mathrm{e}\sin\phi \tag{10.37}$$

Superluminal Motion, IX

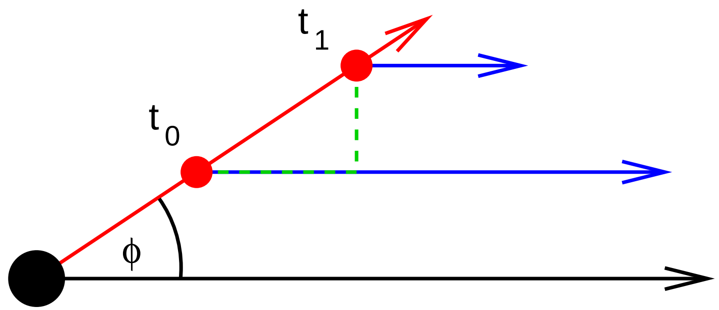

Apparent velocity deduced from observations:

$$v_\mathrm{app} = \frac{\Delta\ell_\perp}{\Delta t_\mathrm{o}} = \frac{v\Delta t_\mathrm{e}\sin\phi}{\left(1 - \frac{v}{c}\cos\phi\right)\Delta t_\mathrm{e}} = \frac{v\sin\phi}{\left(1 - \frac{v}{c}\cos\phi\right)} \tag{10.38}$$

$\Longrightarrow$ For v/c large and ϕ small: $v_\mathrm{app} > c$

Superluminal Motion, X

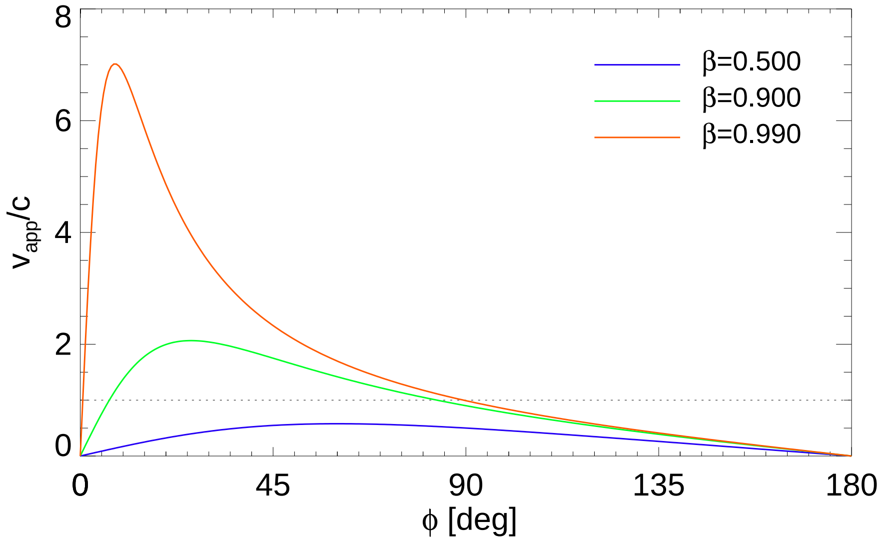

Relativistic Boosting, I

If jet plasma is moving at relativistic speeds, we have to consider also other relativistic effects.

Remember that

$$\nu = \frac{1}{\Delta t_{\mathrm{A}}} = \frac{\nu'}{\gamma\left(1-\frac{v}{c}\cos\theta\right)} \tag{10.39}$$

and

$$\gamma = \frac{1}{\sqrt{1-\frac{v^2}{c^2}}} \quad . \tag{10.40}$$

This defines the relativistic Doppler factor

$$\mathcal{D} = \frac{1}{\gamma\left(1-\frac{v}{c}\cos\theta\right)} = \frac{\sqrt{1-\beta^2}}{1-\beta\cos\theta} \tag{10.41}$$

(the difference to the classical Doppler factor is only the γ factor).

The Doppler factor is a strong function of the aspect angle and can become very large for $v \longrightarrow c$.

Relativistic Boosting, II

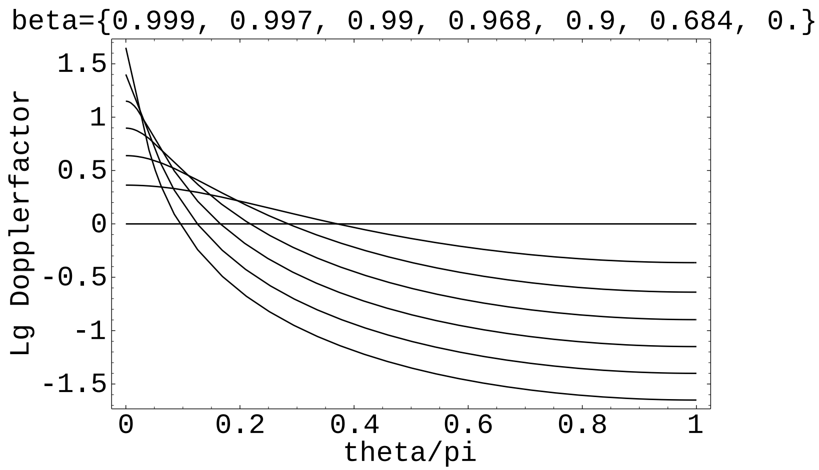

Within $\sim 1-2$ deg, the Doppler factor can approach values of 100 or higher.

Relativistic Boosting, III

One can show (i.e., Rybicki & Lightman, chap. 4.9) that S_ν/ν^3 is invariant under Lorentz transformation, where S_ν is the flux density.

Therefore, observed intensity of a moving blob:

$$\frac{S(\nu_{\mathrm{obs}})}{\nu_{\mathrm{obs}}^3} = \frac{S(\nu_{\mathrm{em}})}{\nu_{\mathrm{em}}^3} \tag{10.42}$$

and

$$S(\nu_{\mathrm{obs}}) = \nu_{\mathrm{obs}}^3 \frac{S(\nu_{\mathrm{em}})}{\nu_{\mathrm{em}}^3} = \mathcal{D}^3 S(\nu_{\mathrm{em}}) \tag{10.43}$$

Specifically, for a blob with a power law spectrum ($S(\nu) = A\nu^\alpha$):

$$S(\nu_{\mathrm{obs}}) = \mathcal{D}^3 A \nu_{\mathrm{em}}^\alpha = \mathcal{D}^3 A \mathcal{D}^{-\alpha} \nu_{\mathrm{obs}}^\alpha \tag{10.44}$$

$$S(\nu_{\mathrm{obs}}) = \mathcal{D}^{3-\alpha} S(\nu_{\mathrm{em}}) \quad . \tag{10.45}$$

Even for relatively modest relativistic velocities of $0.97c$ ($\gamma \simeq 4$), for example, the flux in the forward direction can be boosted by a factor 1000, while it is reduced by a factor 1000 in the backward direction!

Jet One-Sidedness, I

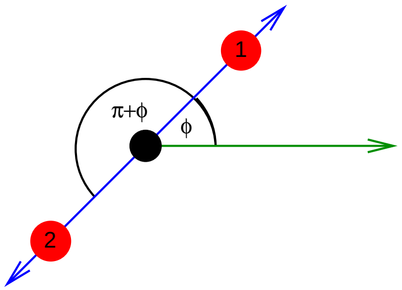

Now take a source emitting blobs symmetrically in two directions.

From Eq. (10.44) the ratio of fluxes from the blobs is

$$\frac{S_1}{S_2} = \left(\frac{1+\beta\cos\phi}{1-\beta\cos\phi}\right)^{3-\alpha} \tag{10.46}$$

Even for mildly relativistic speeds and large angles, features on the approaching side are always significantly brighter than on the receding side.

Jet can be expressed as a series of blobs. But the number of blobs observed scales as the Doppler factor, such that for jets:

$$\frac{S_1}{S_2} = \left(\frac{1+\beta\cos\phi}{1-\beta\cos\phi}\right)^{2-\alpha} \tag{10.47}$$

One sidedness of jets is a relativistic effect!

Survey and monitoring of extragalactic jets on parsec scales with the VLBA since 1995

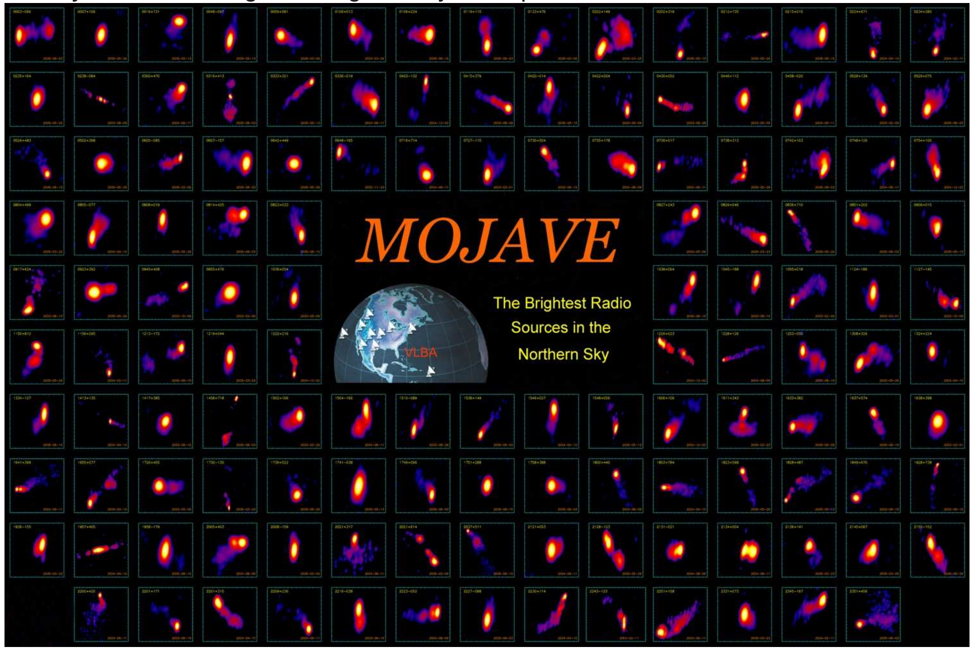

`http://www.physics.purdue.edu/astro/MOJAVE/`

Jet One-Sidedness, II

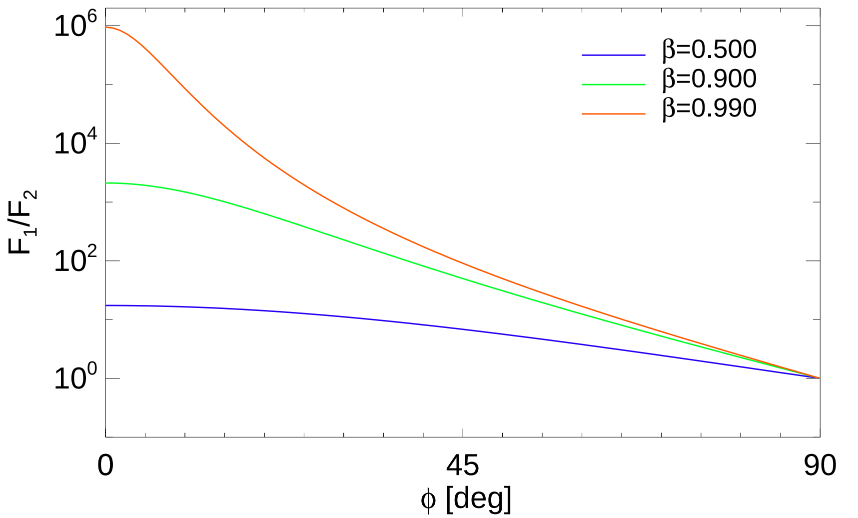

Kinematics of Relativistic Jets on Parsec Scales

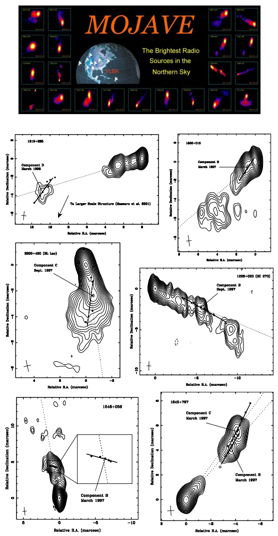

- **MOJAVE**: **M**onitoring **O**f **J**ets in **A**ctive galactic nuclei with **V**LBA **E**xperiments; (Lister et al., 2009)
- Wavelength $\lambda = 2\,\mathrm{cm}$ (15 GHz)
- Statistically complete sub-sample: All flat-spectrum ($\alpha < 0.5$) sources whose compact flux density ever reached 1.5 Jy (2 Jy for southern sources)
- Extended sample includes all known gamma-ray blazars (newly detected *Fermi* sources added since 2009)
- Results, images and movies at `http://www.physics.purdue.edu/astro/MOJAVE/`
- Observing strategy optimized for each individual source (fast sources are observed every month, slower sources less frequently)

Kinematics of Relativistic Jets on Parsec Scales

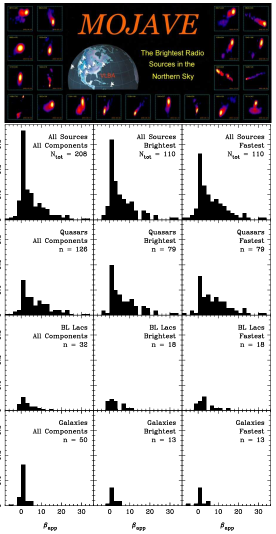

MOJAVE Results:

- Distribution of observed velocities typically between 0 and 15c: Quasars: tail up to $\beta_{\text{app}} \sim 50$; BL Lacs and galaxies: mainly $\beta \lesssim 6$
- In the same jet, different components tend to have similar speeds; but there are exceptions
- In many sources, bent trajectories are seen, which do not back-extrapolate to the core: no cannon-balls!
- Observed pattern speed does not necessarily agree with beam speed
- Most of the flux-density originates in still unresolved regions smaller than 0.05 mas
- High-energy (gamma-ray) emitters have faster and more compact jets

(Kellermann et al., 2004; Kovalev et al., 2005; Cohen et al., 2007)

Overview

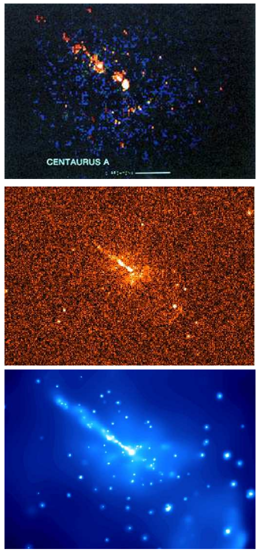

First imaging X-ray observations of jets with *Einstein* (1978-81)
Later *ROSAT* (1990-99)
Golden Era: *Chandra* (1999-present)
Now, $\sim$ 50 X-ray jets known.

Top: *Einstein*: Smithsonian Institution Photo No. 80-16249
Middle: *ROSAT*:
`http://www.mpe.mpg.de/Highlights/FB1997/h97-2-12.ps`
Bottom: *Chandra*: Chandra press release 2001-11-23

Visit the X-Jet homepage:
`http://hea-www.harvard.edu/XJET/`

X-Ray Jets in FR I Galaxies, I

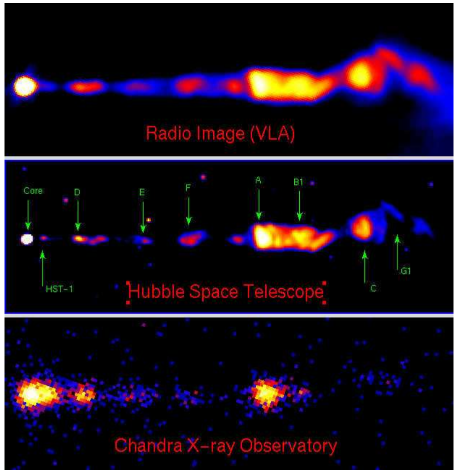

M 87 – Credit: X-ray: NASA/CXC/MIT/H.Marshall et al., Radio: F.Zhou, F.Owen (NRAO), J.Biretta (STScI), Optical: NASA/STScI/UMBC/E.Perlman et al.)

Synchrotron process dominates the broadband spectrum:

- Similar morphologies in the radio, optical, X-ray.
- X-ray spectral index α_X typically steeper than in the radio
- Correlated variability.

Electrons of energies in the range $10^7 < \gamma < 10^8$ are needed.

Common assumption:
Particle acceleration in relativistic shocks.

X-Ray Jets in FR I Galaxies, II

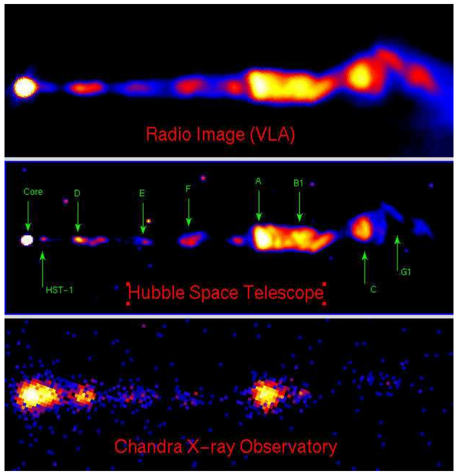

M 87 – Credit: X-ray: NASA/CXC/MIT/H.Marshall et al., Radio: F.Zhou, F.Owen (NRAO), J.Biretta (STScI), Optical: NASA/STScI/UMBC/E.Perlman et al.)

Remember Life-time of particles of energy E is

$$t_{1/2} = 1.6 \times 10^7\,\text{years} \left(\frac{B}{10^{-7}\,\text{T}}\right)^{-2} \gamma^{-1} \tag{10.48}$$

X-ray synchrotron radiating electron of $\gamma = 10^7$ cool on time scales of years.
$\Rightarrow$ Emission regions cannot be much larger than acceleration regions.

Easy to fulfil for compact cores and even for jet knots, but continuous emission between the knots are problematic.

Electron acceleration may take place continuously, e.g., through turbulence in an outer shear layer (Stawarz & Ostrowski, 2002).

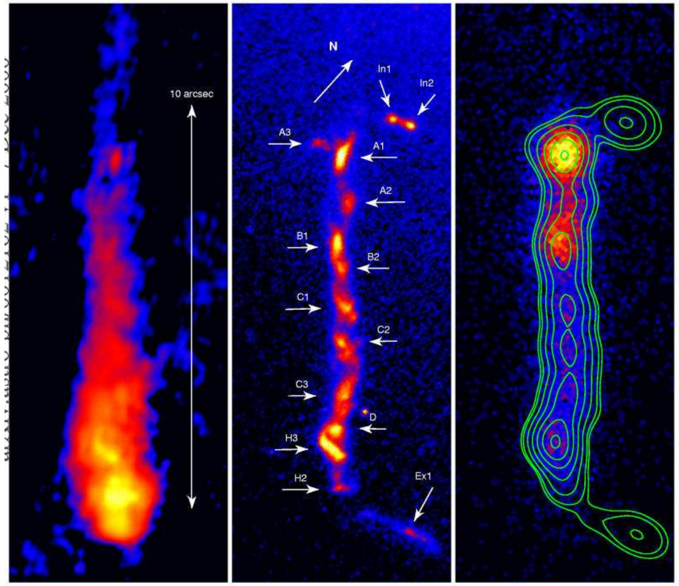

3C 273 – left: radio, 1.6 GHz (MERLIN); middle: optical, F622W filter (HST); right: X-rays, (0.5-8.0) keV (*Chandra*); (Marshall et al., 2001)

X-Ray Jets in FR II Galaxies, II

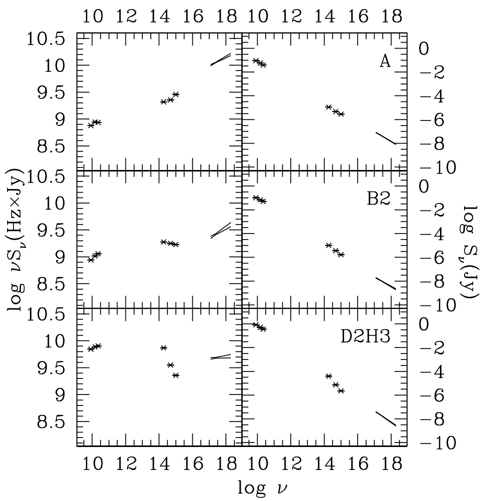

(Harris & Krawczynski, 2006)

The jet of 3C 273 is an example for the "bow-tie problem" in FR II jets: Measured X-ray spectral slopes do not permit a smooth fit with the broadband

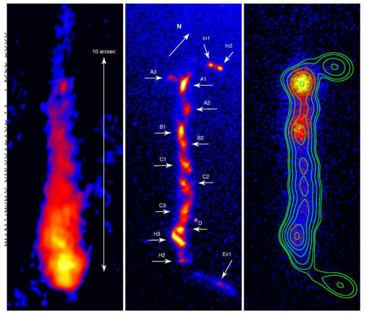

(Marshall et al., 2001)

X-Ray Jets in FR II Galaxies, III

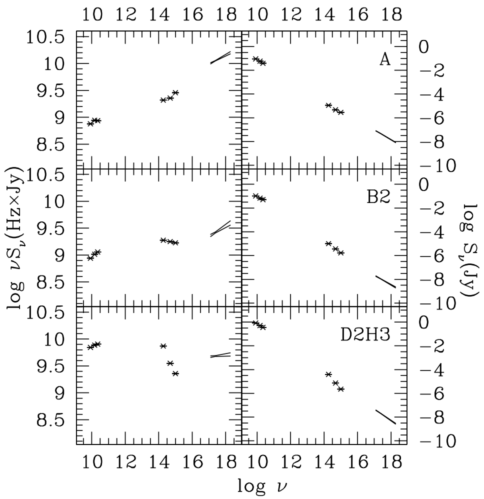

(Harris & Krawczynski, 2006)

The jet of 3C 273 is an example for the "bow-tie problem" in FR II jets: Measured X-ray spectral slopes do not permit a smooth fit with the broadband spectral data.

Need another process to explain FR II X-ray jet emission.

This is more common in FR II jets, but some FR Is have "bow-tie problems", as well.

X-Ray Jets in FR II Galaxies, IV

In relativistic jets, high-energy electrons are all around.

Physical process: Inverse Compton Scattering

Seed photons from

- the primary synchrotron photons of the jet emission: SSC – Synchrotron Self Compton emission (compact jets)
- an external photon field: EC – External Compton emission, e.g., from the cosmic microwave background (IC/CMB models: large-scale jet knots)

The most pressing problem in the context of large-scale extragalactic X-ray jets is whether or not the IC/CMB process is the dominant for high-power FR II and quasar jets or if (modified) synchrotron models can explain the observations.

X-Ray Jets in FR II Galaxies, V

It can be shown that the net power gain of the photon field is

$$P_{\text{compt}} = \frac{4}{3}\sigma_{\text{T}} c\gamma^2\beta^2 U_{\text{rad}} \quad (10.49)$$

Power emitted by synchrotron radiation in a B-field of energy density U_{B} was

$$P_{\text{synch}} = \frac{4}{3}\sigma_{\text{T}} c\gamma^2\beta^2 U_{\text{B}} \quad (10.10)$$

Magnetized plasma: synchrotron photons are inverse Compton scattered by the electrons. Ratio of emitted powers:

$$\frac{P_{\text{compt}}}{P_{\text{synch}}} = \frac{U_{\text{rad}}}{U_{\text{B}}} \quad (10.50)$$

Consequence of the fact that (in QED) synchrotron radiation is inverse Compton scattering off virtual photons of the B-field.

In very compact sources (next lecture), $U_{\text{rad}} > U_{\text{B}}$ is possible, so that $P_{\text{compt}} > P_{\text{synch}}$

$\Longrightarrow$ (synchrotron) photon field will undergo dramatic amplification

$\Longrightarrow$ very efficient cooling of electrons by inverse Compton losses (Compton catastrophe).

As a result, the brightness temperature of **compact** radio sources is limited to 10^{12} K.

Relativistic Bulk Motion on Kpc Scales, I

Bulk relativistic jet motion needed on kpc scales in order to explain IC/CMB emission

- Apparent superluminal motion remains the clearest signature of bulk relativistic motion
- Well established on parsec scales with VLBI but difficult to measure on kpc scales because of a lack of sufficiently compact features
- Optical telescopes (HST) have supperior angular resolution compared to *Chandra*

Superluminal motion in M 87: (Biretta, Sparks & Macchetto, 1999)

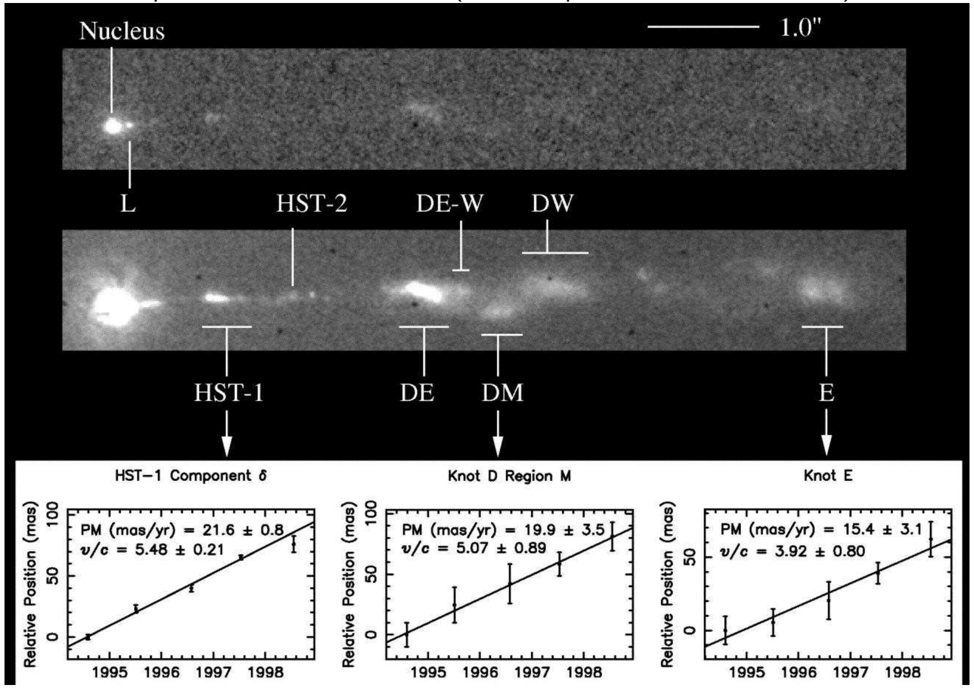

Relativistic Bulk Motion on Kpc Scales, III

Superluminal motion in M 87: (Biretta, Sparks & Macchetto, 1999)

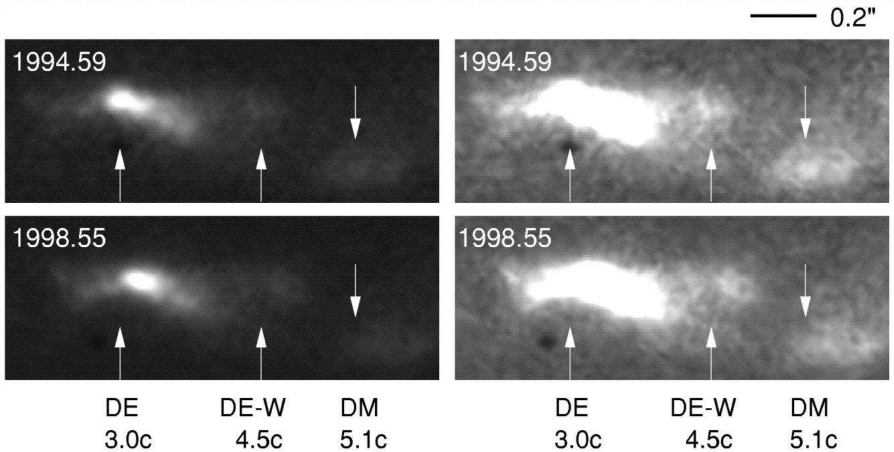

Note that MOJAVE measures only 0.05 c at 2 cm on milliarcsecond scales.

Relativistic Bulk Motion on Kpc Scales, IV

Superluminal motion in M 87: (Biretta, Sparks & Macchetto, 1999)

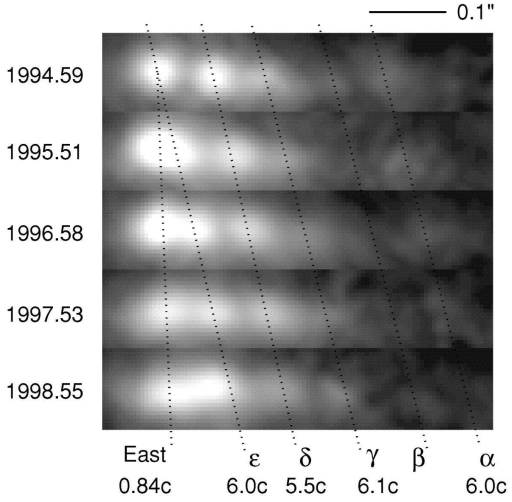

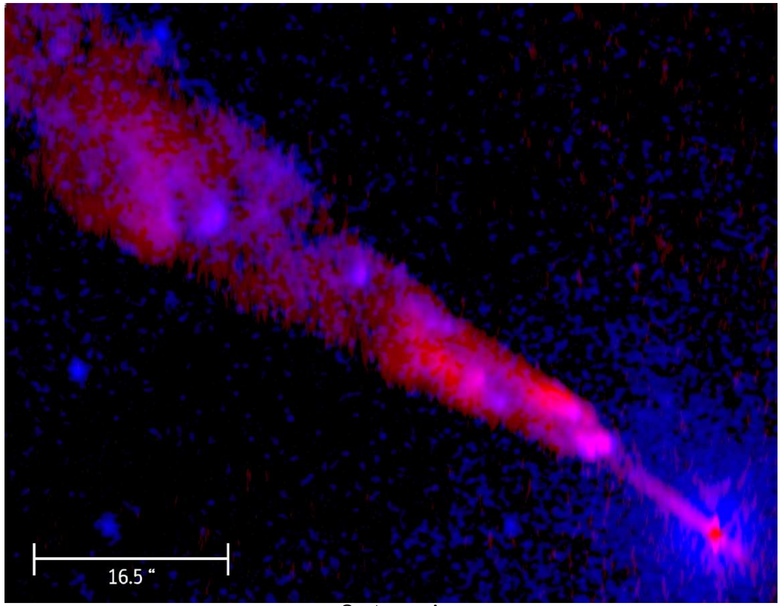

Centaurus A

Credit: X-ray: NASA/CXC/Bristol U./M. Hardcastle et al.; Radio: NRAO/AUI/NSF/Bristol U./M. Hardcastle

Misalignments of Radio-, Optical-, X-Ray Jet Features, I

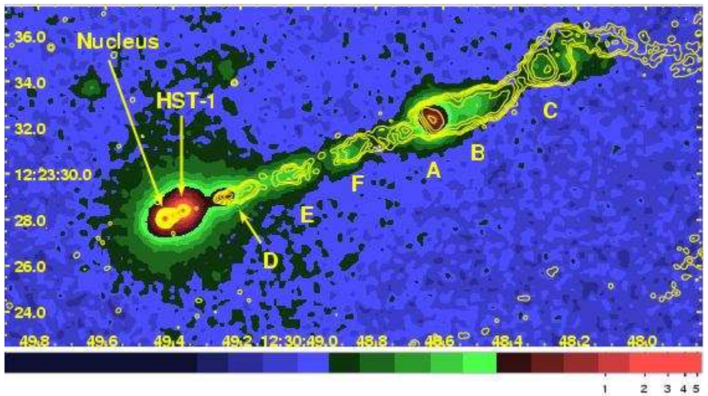

(Harris & Krawczynski, 2006)

Radio jet "circumnavigates" around an obstacle beyond knot C.
X-ray emission may come from the obstacle rather than from the jet itself.
There are offsets between radio and X-ray peaks in knots D and F.

Misalignments of Radio-, Optical-, X-Ray Jet Features, III

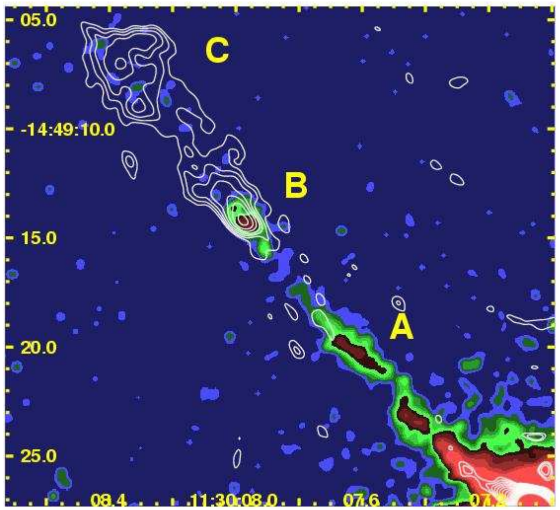

PKS 1127-145 (*Chandra*/VLA) – (Harris & Krawczynski, 2006)

- In nearby sources (Cen A, M 87), offsets are of the order of tens of parsecs
- In PKS 1127-145 ($z = 1.18$), the offset in knot B is 10 kpc.
- Resolution effects combined with radiative losses during downstream motion
- Alternatively, the radio emissivity may be enhanced downstream from a shock region
- Offsets in IC/CMB knots are much more difficult to explain

Misalignments of Radio-, Optical-, X-Ray Jet Features, IV

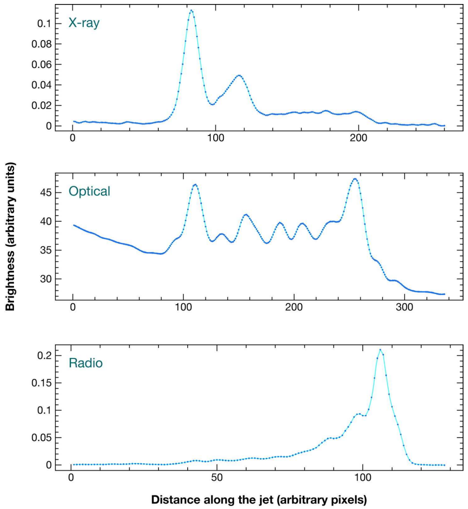

Profiles along the jet in 3C 273 – (Harris & Krawczynski, 2006)

- X-ray intensity often highest at the upstream end, whereas the radio intensity increases downstream: **Progressions**
- Common effect, most prominent in 3C 273
- Degraded angular resolution (or larger distance) would create an offset
- Progressions can be explained via increasing magnetic field strengths in synchrotron jets and via jet deceleration in IC/CMB jets.

Outlook

In IC/CMB models, the X-rays are produced from low-energy electrons from the bottom of the energy distribution. Their primary synchrotron emission would lie well below the frequencies probed until today.

Tests of synchrotron vs. IC/CMB models:

- Look for a cutoff at high X-ray energies
- Observe the IC/CMB seed-electrons in the radio: their low-frequency ($\sim$ 100 MHz) emission will be detectable with LOFAR and the LWA.
- More and deeper optical/IR observations to show if this emission is from the top end of the synchrotron spectrum or the bottom of the IC component.
- Model sensitivity of 5-yr *Fermi* all-sky survey predicts that the putative IV/CMB of many FR II knots should be detectable at GeV energies (Dermer & Atoyan, 2004); Problem: angular resolution.
- Search for signals at even higher energies (TeV range: H.E.S.S., MAGIC, VERITAS, CANGAROO); better angular resolution but; Problem: universe not transparent at high redshifts

Introduction, I

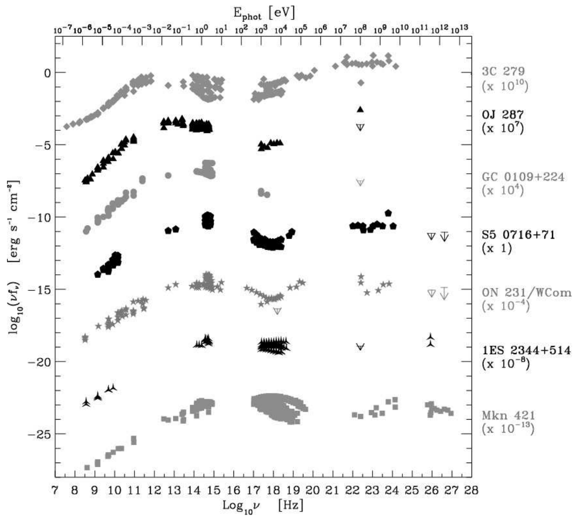

(Fiorucci, Ciprini & Tosti, 2004)

Blazars emit across the whole electromagnetic spectrum!

We have seen images of the powerful relativistic parsec-scale jets of blazars before. How can we transfer the power of the compact jet into high-energy emission?

Introduction, II

Blazars are broadband emitters and the most natural targets for multiwavelength astronomy!

The expression *Blazar* was first used in 1978 to express that optically violently variable quasars (OVVs) and BL Lac objects share their extreme variability characteristics.

Although been first detected in the optical and radio, a large portion of their total energy output is at high energies: hard X-rays, γ-rays, and up to the very high energy (VHE) regime.

γ-ray telescopes like *Fermi* find that blazars are the dominant population of extragalactic γ-ray sources.

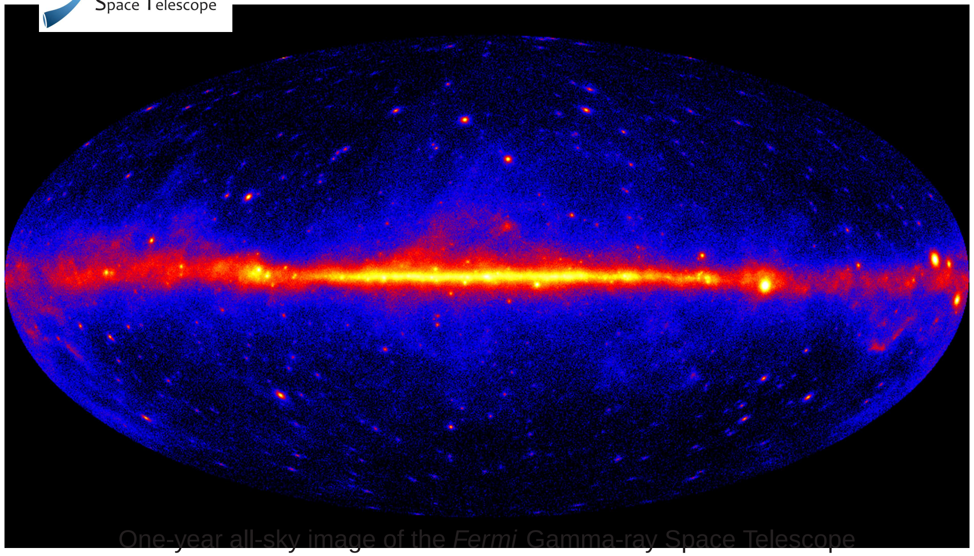

One-year all-sky image of the *Fermi* Gamma-ray Space Telescope (2008/09)

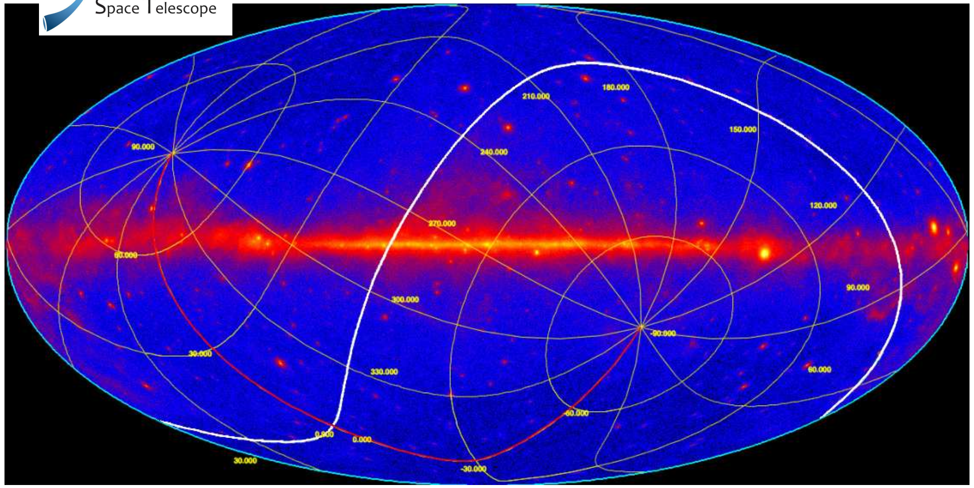

All-sky astronomy is tricky from the ground!

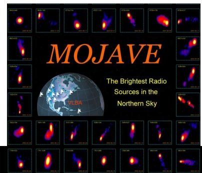

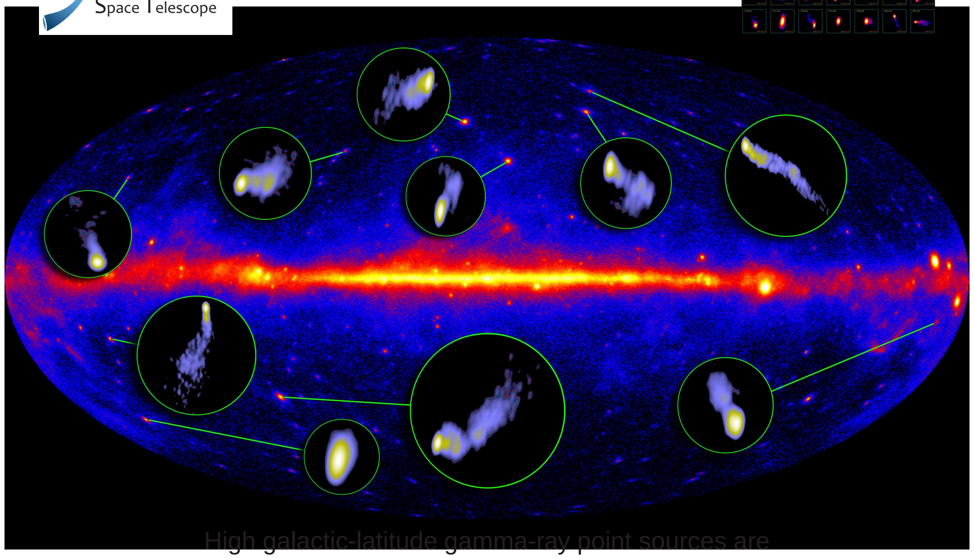

High galactic-latitude gamma-ray point sources are flat-spectrum radio quasars and BL Lac objects

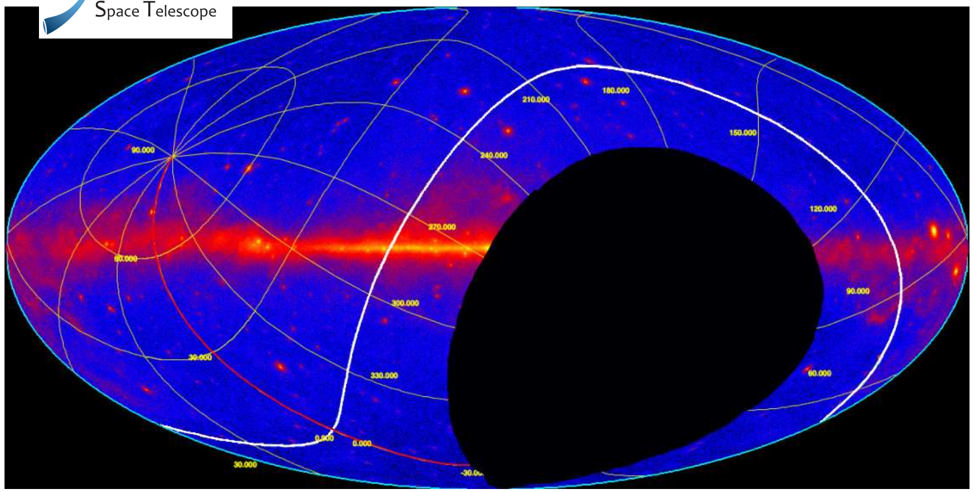

One third of the sky is not observable for Northern-Hemisphere Telescopes!

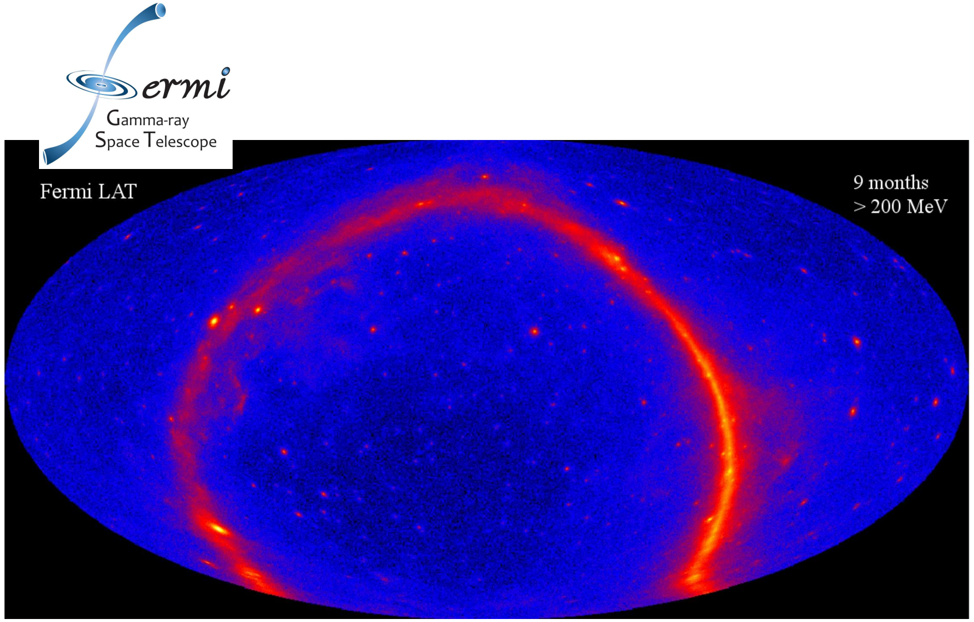

All-sky *Fermi* γ-ray image in celestial coordinates

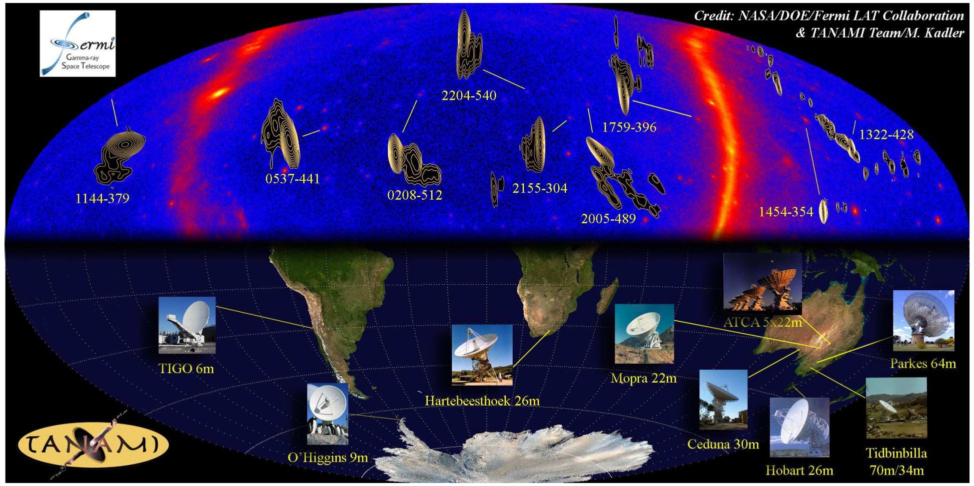

TANAMI (Tracking Active Galactic Nuclei with Austral Milliarcsecond Interferometry)
`http://pulsar.sternwarte.uni-erlangen.de/tanami`

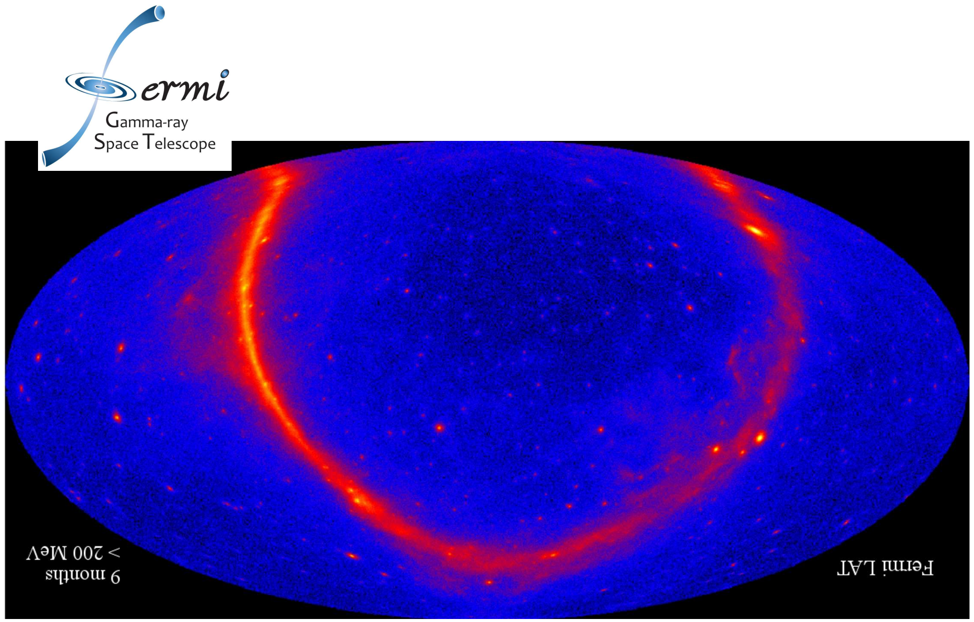

Austral View of *Fermi* γ-ray sky

Introduction, X

Blazars are extremely variable on time scales as short as days! $\Rightarrow$ Source dimensions $R \sim \mathcal{O}(10^{10}\,\mathrm{m})$

High photon density n_γ may enable pair production:

$$\gamma + \gamma \rightarrow e^- + e^+ \tag{10.51}$$

if $E_\gamma > \mathrm{m}_e c^2 = 511\,\mathrm{keV}$.

Optical depth for pair production:

$$\tau_{\gamma\gamma} = n_\gamma \sigma_{\gamma\gamma} R, \tag{10.52}$$

with $\sigma_{\gamma\gamma}$ the cross section for pair production (close to the Thomson cross section σ_T close to the energy threshold).

n_γ from energy density $(L_\gamma/4\pi R^2 c)$ divided by mean energy $(m_e c^2)$. Therefore:

$$\tau_{\gamma\gamma} \sim \left(\frac{L_\gamma}{4\pi R^2 m_e c^3}\right) \sigma_\mathrm{T} R \sim 200 \left[\frac{L_\gamma}{10^{48}\,\mathrm{erg\,s^{-1}}}\right] \left[\frac{R}{10^{10}\,\mathrm{m}}\right], \tag{10.53}$$

i.e., photons cannot escape, unless L_γ is emitted non-isotropically.

Short time scales and high γ-ray luminosities provide and independent proof of relativistic beaming in blazar jets.

The Blazar Sequence

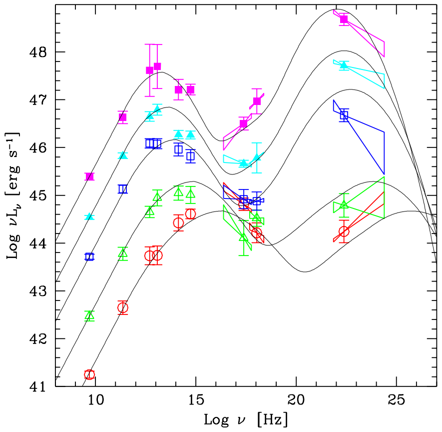

Construction of average blazar SEDs binned according to radio luminosity (Fossati et al., 1998; Donato et al., 2001)

- For all luminosity classes, two broad peaks
- High-luminosity sources peak at lower frequencies (IR and MeV range): LBL objects
- Low-luminosity sources peak at higher frequencies (UV/X-rays and up to TeV energies): HBL objects

(Donato et al., 2001, based on Fossati et al. (1998))

The Blazar Sequence

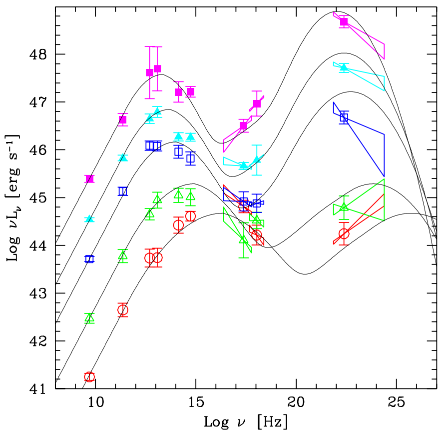

Analytic parametrization:

- Peak frequencies are inversely proportional to luminosity
- Constant ratio of the two peak frequencies
- Strength of the second peak proportional to luminosity

Attention: EGRET detected preferentiall blazars during outbursts ⇒ Bias in high-energy data.

Ongoing debate about the validity of the blazar sequence. A (small) number of sources do not fit in.

(Donato et al., 2001, based on Fossati et al. (1998))

Prototypical Example: 3C 273

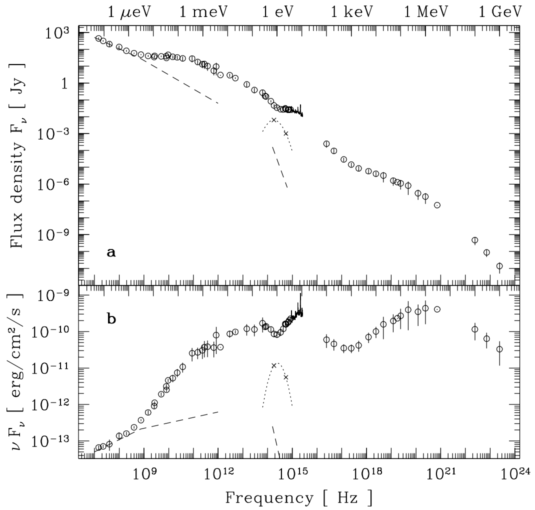

(Türler et al., 1999)

3C 273:

- First detected and brightest (and probably best studied) quasar
- Bright throughout the whole electromagnetic spectrum
- Prominent "big blue bump"
- Huge public database: Türler et al. (1999); Soldi et al. (2008)

Prototypical Example: 3C 273

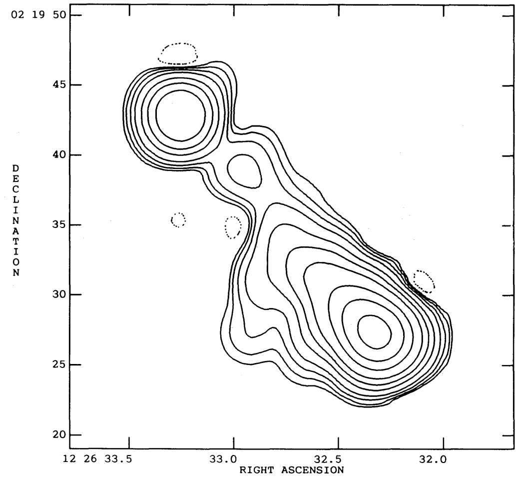

(Conway et al., 1993)

The kpc-scale jet of 3C 273 seen at $\lambda = 198$ cm with MERLIN

Prototypical Example: 3C 273

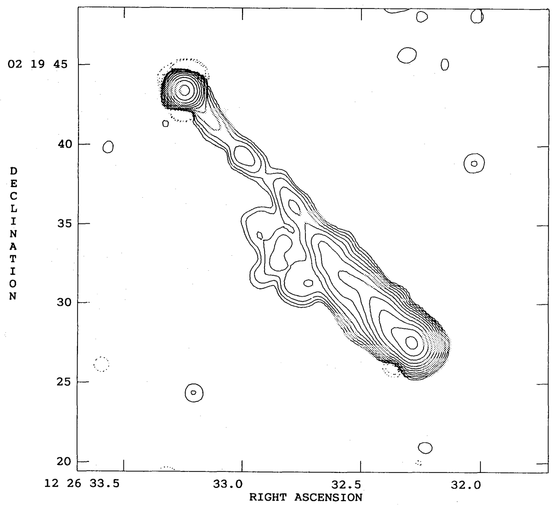

The kpc-scale jet of 3C 273 seen at $\lambda = 73$ cm with MERLIN

(Conway et al., 1993)

Prototypical Example: 3C 273

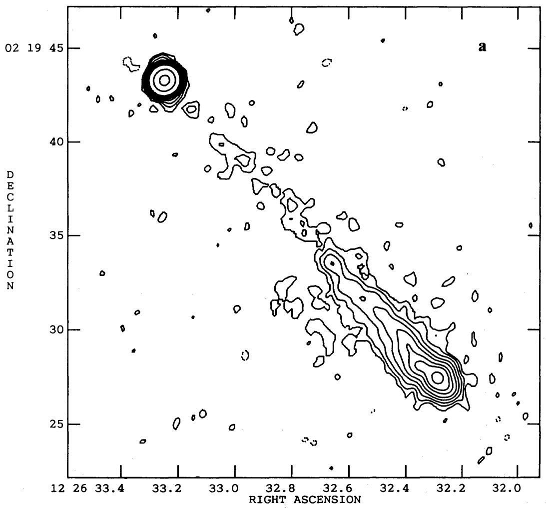

Contribution of large-scale jet negligible above $\sim$ 5 GHz. (Almost) all higher-frequency emission is coming from (sub)-parsec scales.

The kpc-scale jet of 3C 273 seen at $\lambda = 2$ cm with the VLA

(Conway et al., 1993)

Prototypical Example: 3C 273

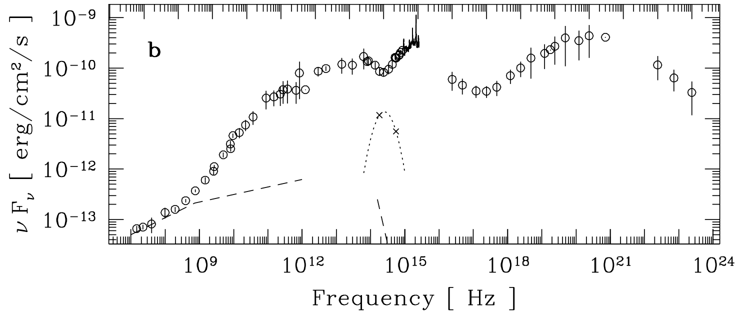

- Radio: low-frequency emission from large-scale jet; high-frequencies from compact jet (flat spectrum in F_ν)
- up to IR: synchrotron emission from compact jet (possibly plus dust component (dusty torus?))
- "big blue bump" in the optical: accretion disk (?)
- X-rays and up: inverse Compton emission (possibly from multiple seed photon fields)

Broadband Emission Models

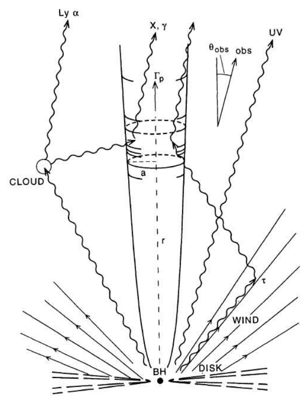

Geometry in leptonic models (Sikora, Begelman & Rees, 1994)

General agreement that the low-energy component is jet-synchrotron emission.

High-energy photons are produced in

- Leptonic models through IC scattering of soft seed photons by the same relativistic electrons responsible for the synchrotron emission. Seed photons are
  - the synchrotron photons themselves (SSC, e.g. Tavecchio, Maraschi & Ghisellini, 1998), or
  - external, e.g., from the accretion disk or the BLR (EC, e.g. Sikora, Begelman & Rees, 1994)
- Hadronic models through reactions involving high-energy protons (hadron-hadron or photon-hadron collisions, pair production and subsequent e^+e^- cascades (e.g. Mannheim, 1993))

Hadronic models are attractive because they can explain the observed ultra-high energetic (UHE) cosmic rays but they have problems explaining the observed blazar X-ray spectra.

Broadband Emission Models

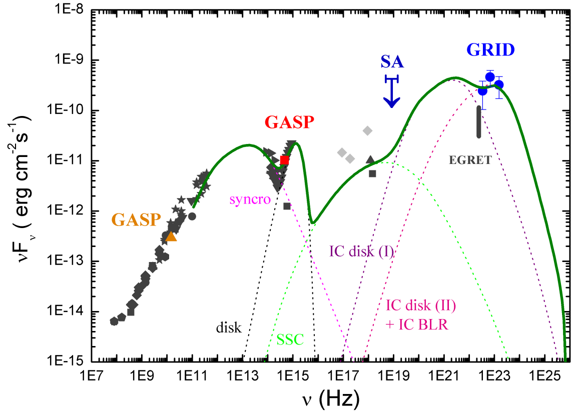

Pucella et al. (2008)

This is an SED of PKS B 1510-089; see below

Modeling the broad-band SED:

- Consider primary components: synchrotron, disk, scattered BLR emission
- Inverse-Compton components from SSC and EC (of the dominating external photon fields)

Prototypical Example: 3C 273 (Blazar Variability), I

Almost 40 years of multiwavelength observations of 3C 273 (Soldi et al., 2008)

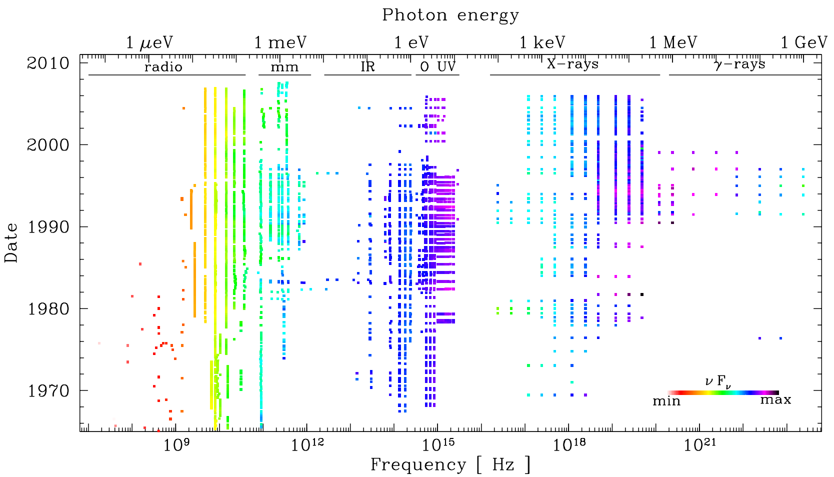

Prototypical Example: 3C 273 (Blazar Variability), II

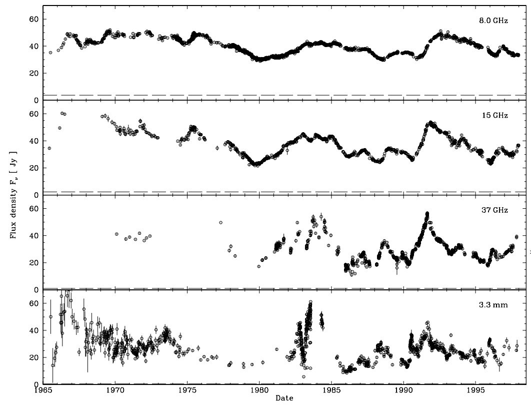

(Türler et al., 1999)

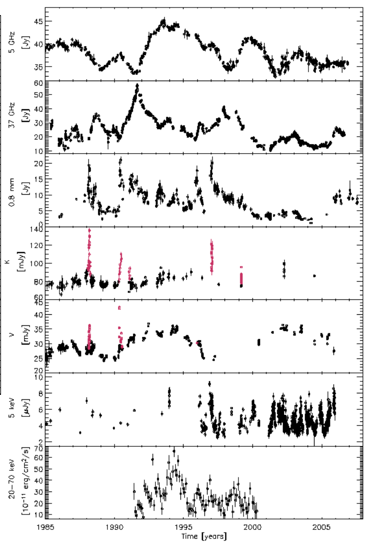

(Soldi et al., 2008)

Variability at all wavelengths but with different time scales and amplitudes ⇒ multiple emission components and/or mechanisms

Prototypical Example: 3C 273 (Blazar Variability), III

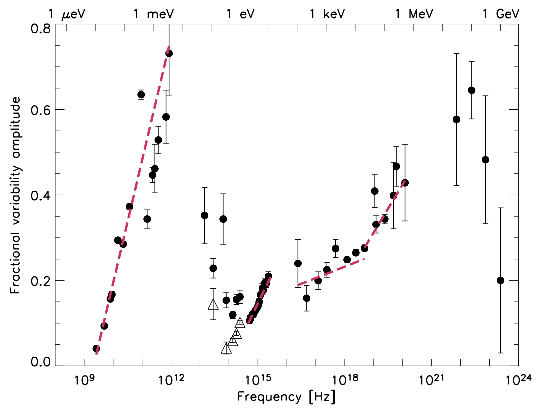

(Soldi et al., 2008)

Fractional variability amplitude:

$$F_{\rm var} = \sqrt{\frac{S^2 - \bar{\varepsilon^2}}{\bar{x}^2}} \quad (10.54)$$

with the sample variance of the light curve S^2, the average flux $\bar{x}$, and the mean of the squared measurement uncertainties $\bar{\varepsilon^2} = \frac{1}{N}\sum_i \varepsilon_i^2$.

The fractional variability amplitude strongly depends on frequency, rising towards the high-energy end of the synchrotron and IC components. Less-variable IR emission (from dust?).

Prototypical Example: 3C 273 (Blazar Variability), IV

Almost 40 years of multiwavelength observations of 3C 273 (Soldi et al., 2008)

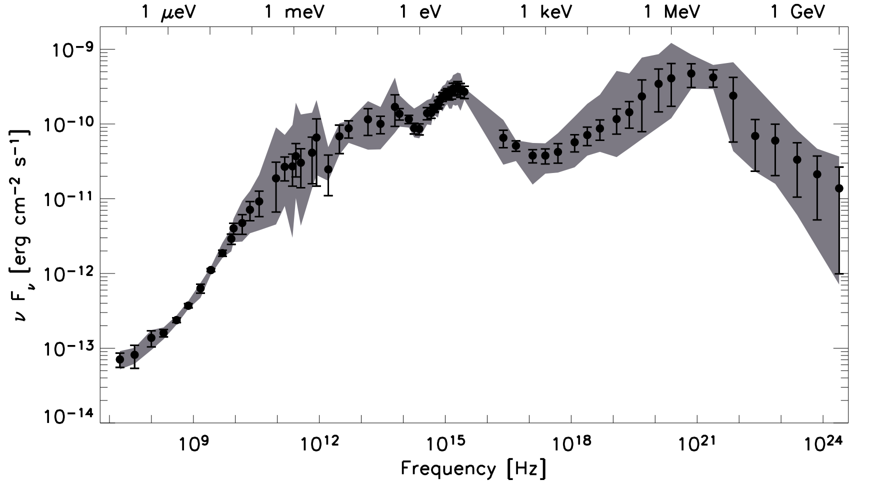

Prototypical Example: 3C 273 (Blazar Variability), V

A historic jet-emission minimum (Türler et al., 2006)

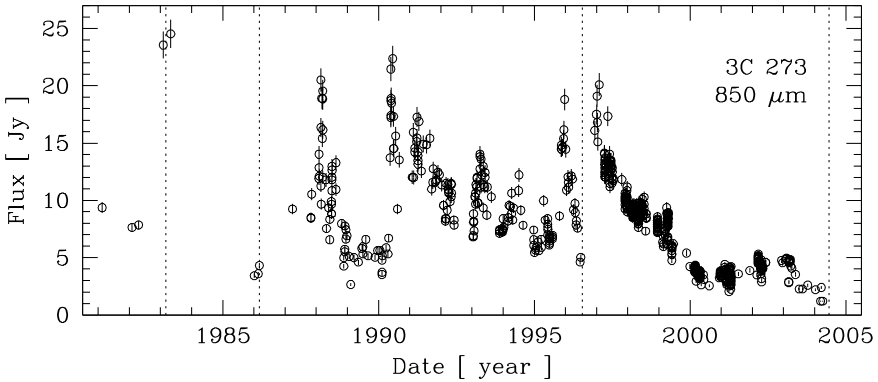

Prototypical Example: 3C 273 (Blazar Variability), VI

A historic jet-emission minimum (Türler et al., 2006)

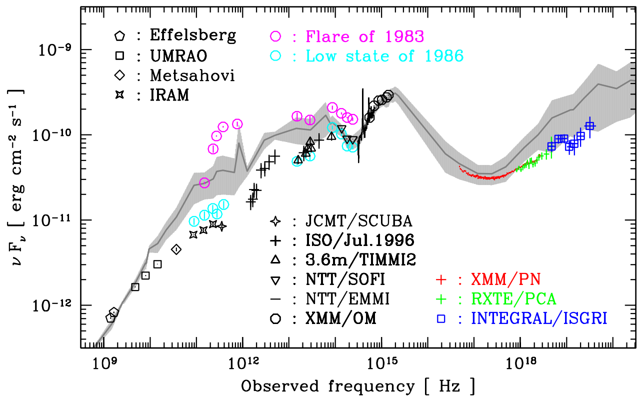

When the jet is weak, Seyfert-like features appear: Thermal dust, iron line; blue bump not directly coupled to jet emission

Prototypical Example: 3C 273 (Blazar Variability), VII

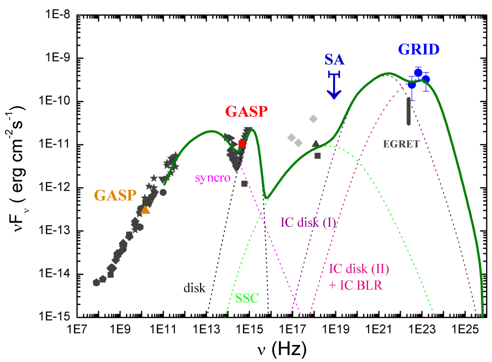

Agile+GASP observation of PKS B1510-089: Pucella et al. (2008)

GASP: GLAST-Agile Support Program

Quasar PKS B1510-089:

- 100 MeV to 1 GeV spectrum: PL with $\Gamma \sim 2$
- SED modeled with a synchrotron+SSC+IC model (external photon field from the disk and from BLR) for a jet with Lorentz factor $\gamma = 20$ observed at the critical angle $1/\gamma$.

MOJAVE speed for 1510-089: $\sim$ 20c!
Maybe even faster at 43 GHz (46 c)

Prototypical Example: 3C 273 (Blazar Variability), VIII

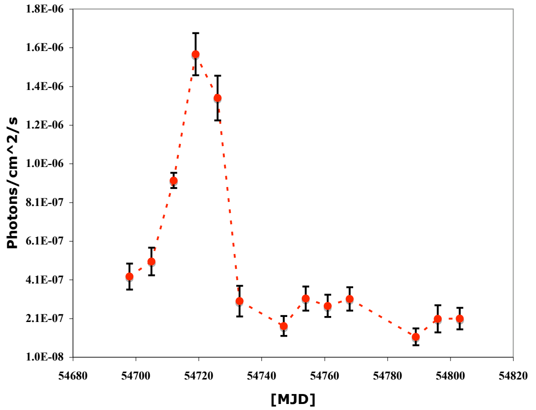

Fermi light curve of PKS B1510-089 (shown are weekly data points starting in late August 2007, about 1 year after the *Agile* pointed observation.)

- Bright flare of 1510-089 detected by *Fermi* in September 2008 (Tramacere, 2008)
- Analysis of follow-up multiwavelength observations going on
- LAT still in calibration phase $\Rightarrow$ only photons/cm^2/s are published

The LAT detector onboard *Fermi* operates in all-sky scanning mode.

With *Fermi* it is now much easier to detect source flares and compare flaring and non-flaring SEDs.

Blazars at Very High Energies

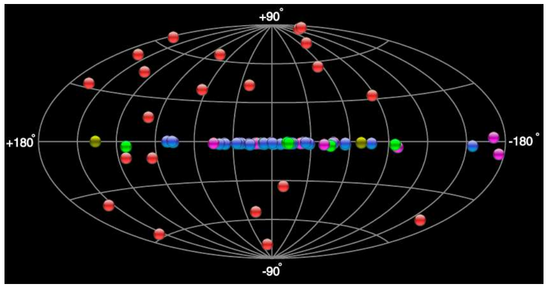

The blazar sequence predicts a dominance of HBL objects at very high energies. This is confirmed by recent blazar detections of TeV telescopes (H.E.S.S., MAGIC, VERITAS, CANGAROO):

- Currently 17 HBL objects detected and only two LBL objects (W Comae and BL Lac; check `http://tevcat.uchicago.edu/` for updated lists)
- Only non-blazar TeV source: M 87

Blazars at Very High Energies

TeV blazars are weak radio sources, because the cm-range is so far left of their synchrotron peak and because they are low-luminosity objects.Similarly, they are bright X-ray sources and relatively weak in the MeV/GeV range.

Despite their variability and SEDs require very high Doppler factors, VLBI measures slow jets (barely superluminal Piner, Pant & Edwards, 2008, and references therein) $\Rightarrow$ 1) extremely small angles or 2) jet deceleration from the "blazar scale" to the "VLBI scale", or 3) another sign of jet-stratification (spine-sheath structure).

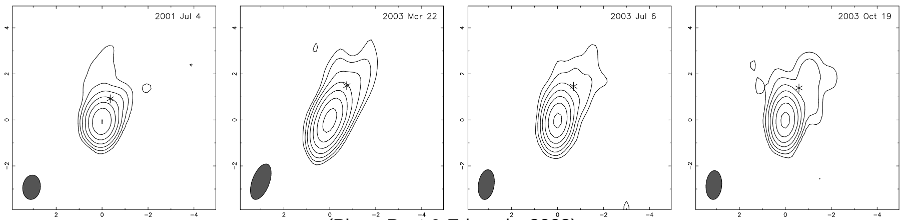

(Piner, Pant & Edwards, 2008)

The Only TeV Galaxy: M 87

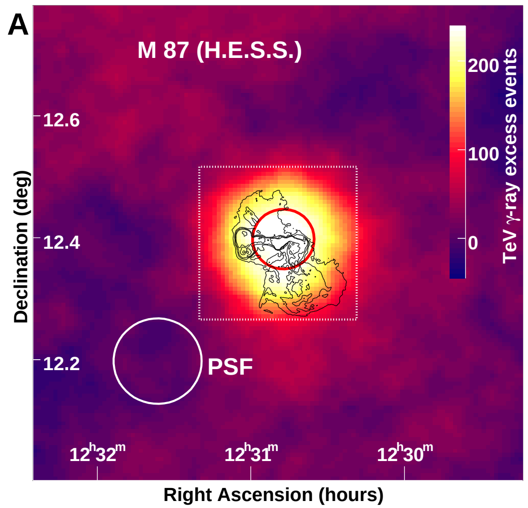

(Aharonian et al., 2006)

- M 87 established as a TeV source by H.E.S.S. (Aharonian et al., 2006)
- Previous 4-σ tentative detection by HEGRA; non-detection by Whipple
- Hard spectrum ($\Gamma \sim 2.2$) detected up to 20 TeV

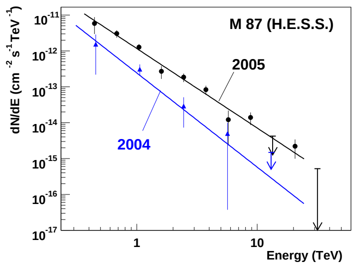

The Only TeV Galaxy: M 87

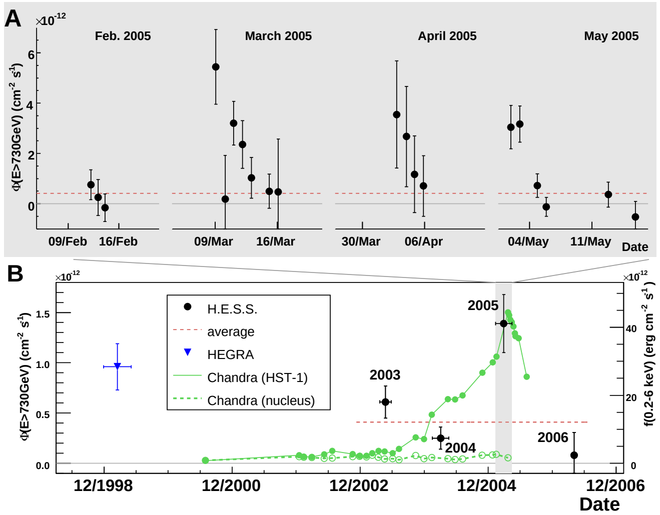

(Aharonian et al., 2006)

- TeV flux variable on time scales from years down to days
- Emission region must be compact
- Highest measured fluxes coincide with a flare of the HST-1 knot in the M 87 jet as measured by *Chandra* (Harris et al., 2006) (at this epoch brighter than the nucleus!)

The Only TeV Galaxy: M 87

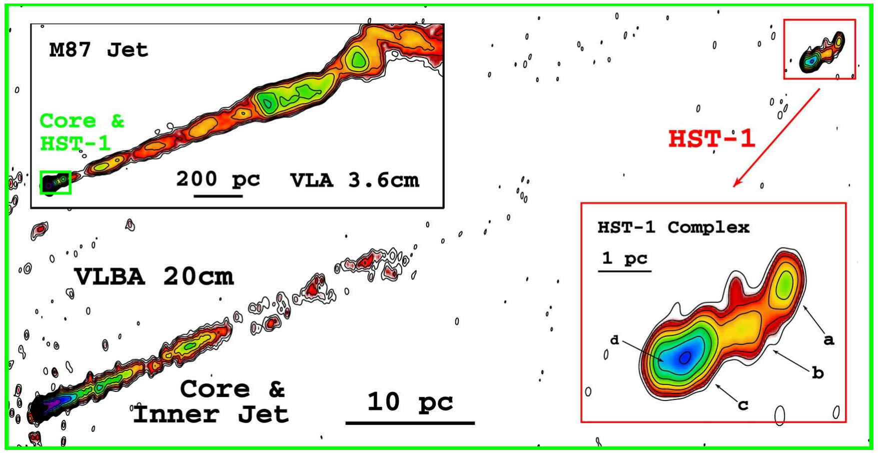

HST-1 resolved by VLBI, but still compact sub-structure (Cheung, Harris & Stawarz, 2007)

The Only TeV Galaxy: M 87

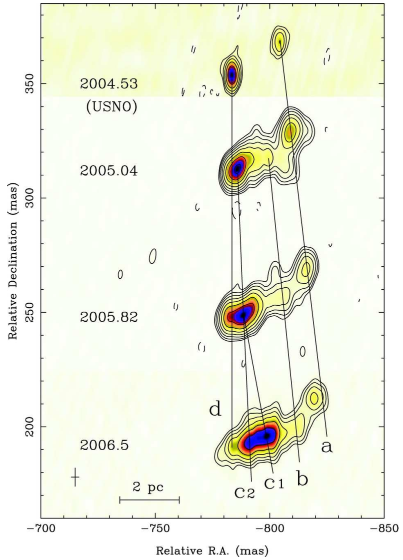

- HST-1 has moving sub-components with super-luminal speeds up to $\sim$ $4c$ in agreement with optical measurements by Biretta, Sparks & Macchetto (1999).

$\Rightarrow$ Relativistic bulk motion $>$ 120 pc downstream from the central engine and coinciding with the flaring putative TeV emission region

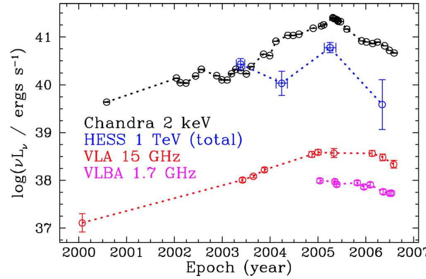

(Cheung, Harris & Stawarz, 2007)

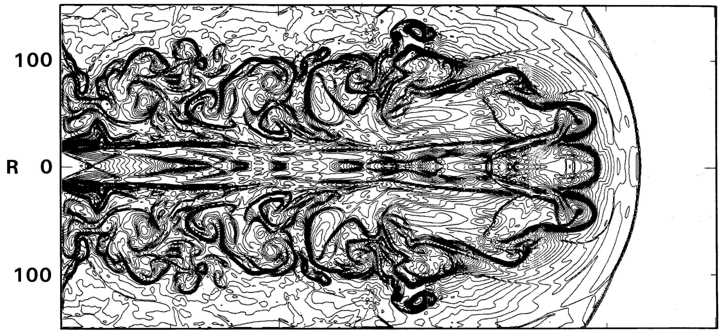

Jet propagation is very difficult hydrodynamics: generally solved numerically

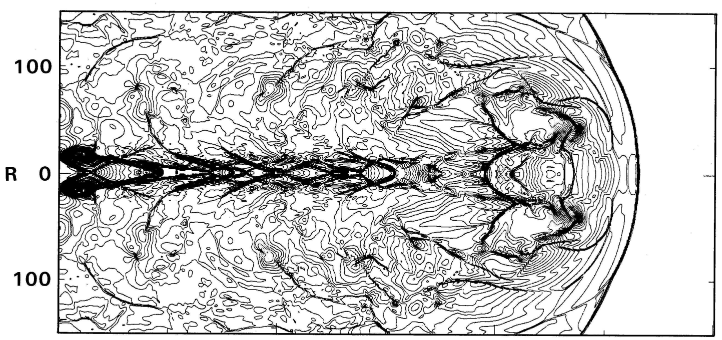

Numerical simulation of a Mach=6 jet (Top: density, bottom: pressure Lind et al., 1989).

Turbulent structure due to Kelvin-Helmholtz instability (hydrodynamical instability in shear flows)

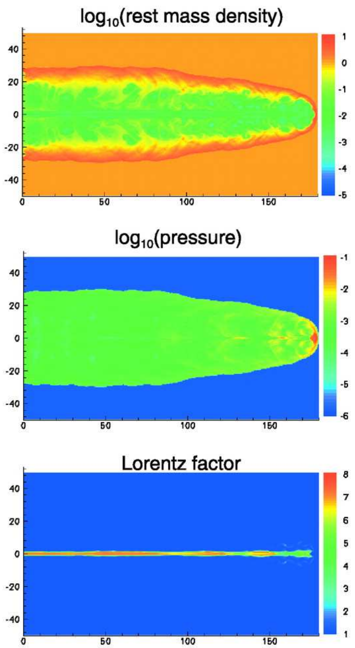

(Mizuta, Yamada & Takabe, 2004)

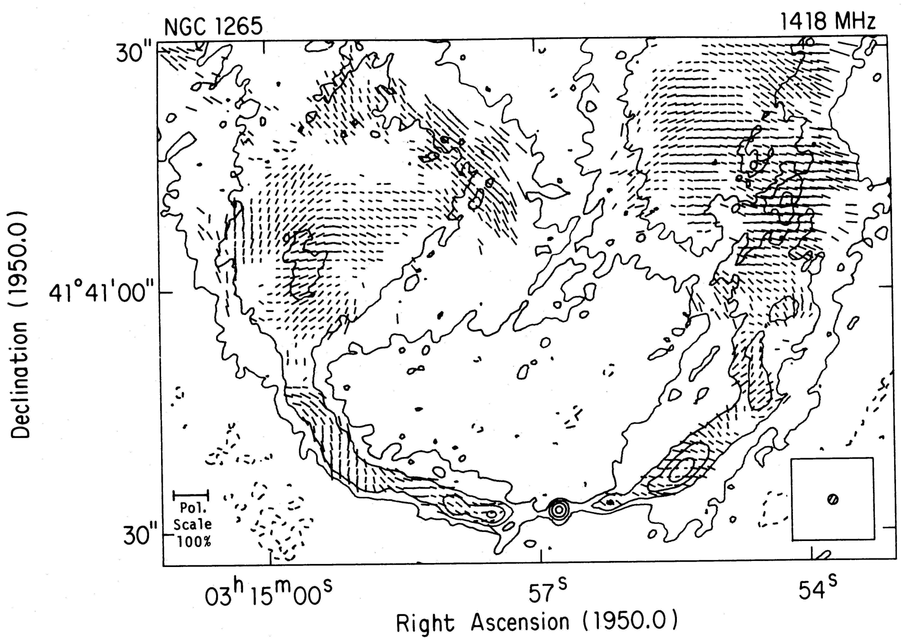

E-field structure of NGC 1265 (**?**)

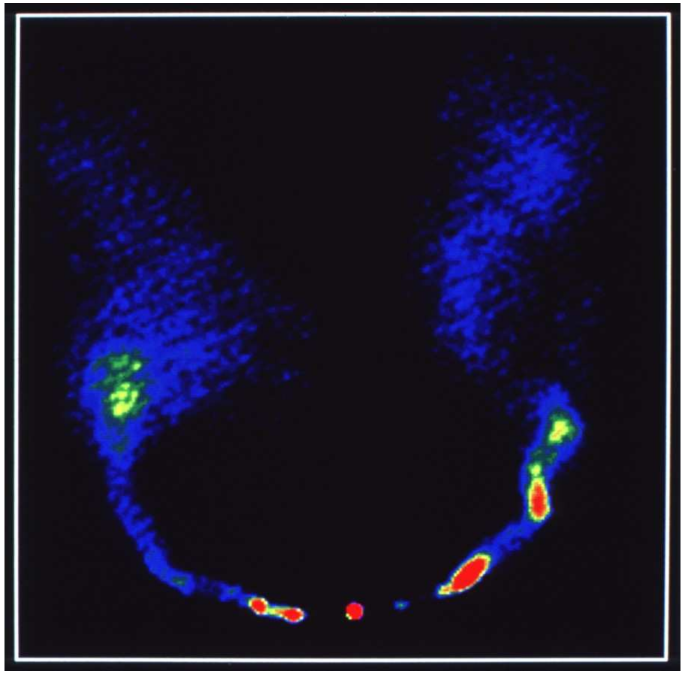

NGC 1265: radio galaxy in Perseus cluster, moving with $2000\,\mathrm{km\,s^{-1}}$ through intergalactic medium.

(NRAO/AUI; **?**)

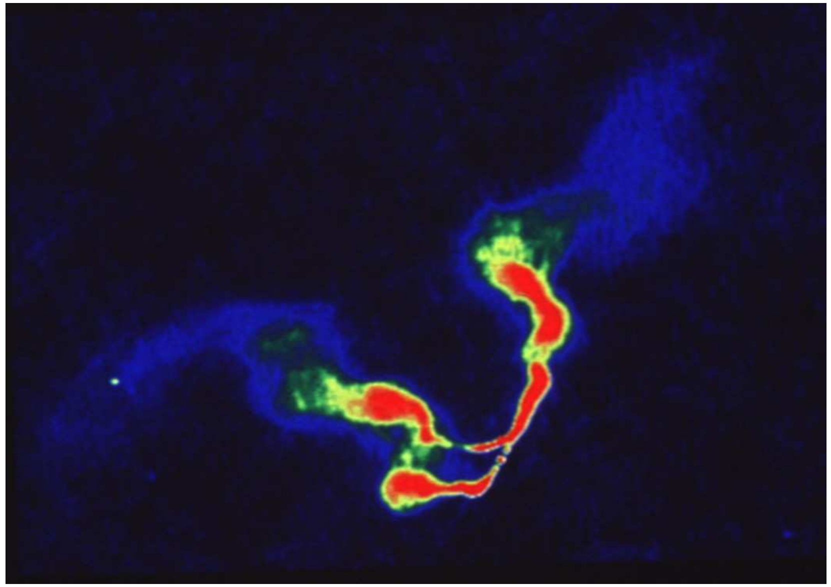

(NRAO/AUI/Owen et al.)

3C75 in Abell 400 at $\lambda = 20\,\mathrm{cm}$: twin radio jets from double core.

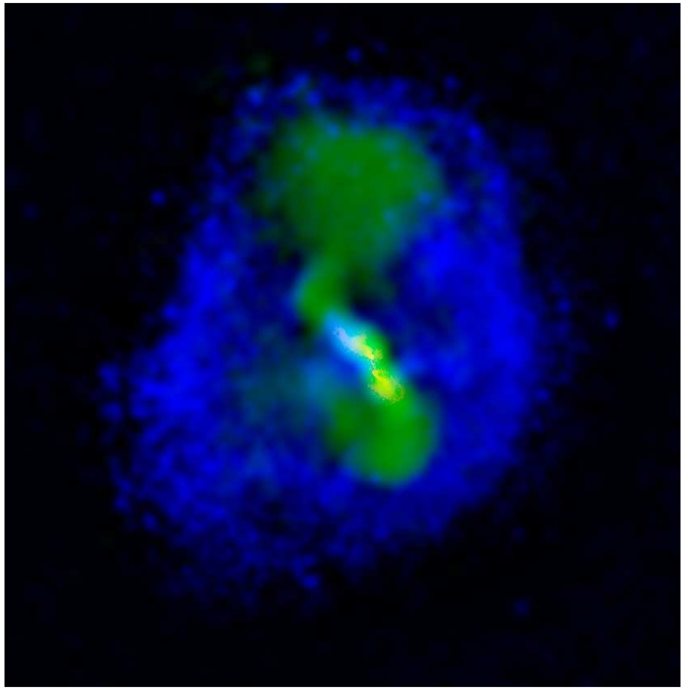

Hydra A: Multiple cavities drifting outwards through the intergalactic medium. Cavity system created in the past 200–500 Myears

green: radio, blue: X-rays, after subtracting elliptical β-model for gas distribution.

Size scale: outer cavities have diameters of 200 and 120 kpc.

(courtesy Mike Wise, UvA, astro-ph/0612100)

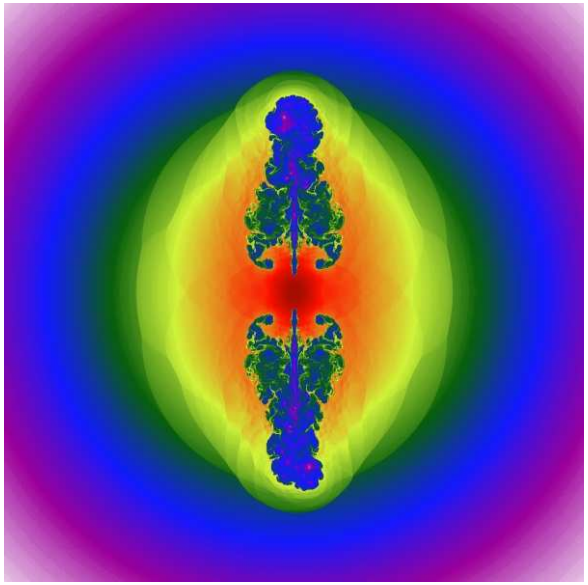

Global view of jet-IGM-interaction and cavity formation

courtesy M. Brüggen (IUB) and UKAFF

Movie: `jetmovies/brueggen_moviebig2.avi`

see Heinz et al., 2006, MNRAS

Formation of jet substructure / cavities in MHD simulations of a jet penetrating into a cluster gas

courtesy M. Brüggen (IUB) and UKAFF

Jets and IGM, VII

Radio lobe physics:

Total energy content of lobe for a power law distribution of electrons, $n(E) = n_0 E^{-p}$:

$$U_\mathrm{e} = V \int_{E_1}^{E_2} n(E)\, E\, dE = \frac{V n_0}{2-p} \left(E_2^{2-p} - E_1^{2-p} \right) \qquad (10.55)$$

Integrating over the synchrotron spectrum (Eq. (**??**)) gives the total synchrotron luminosity produced by this electron population:

$$L = \frac{4\sigma_\mathrm{T} U_B V n_0}{3 m_\mathrm{e}^2 c^4} \left(\frac{E_2^{3-p} - E_1^{3-p}}{3-p} \right) \qquad (10.56)$$

Using the characteristic frequency

$$\omega_\mathrm{c} = \gamma^2 \omega_\mathrm{L} = \frac{eB}{m_\mathrm{e} c} \left(\frac{E}{m_\mathrm{e} c^2} \right)^2 \qquad (10.16)$$

E_1 and E_2 can be expressed in terms of the frequency band over which the power law is observed, ν_1, ν_2. After some messy calculation one obtains:

$$\frac{U_\mathrm{e}}{L} = \frac{A}{B^{3/2}} \qquad (10.57)$$

where A is some constant.

Jets and IGM, VIII

The total kinetic energy in particles is

$$U_{\text{particles}} = aU_{\text{e}} = aAB^{-3/2}L \tag{10.58}$$

where $a > 1$ (since there are other particles than electrons in the lobe).

Therefore the total energy of the radio lobe is

$$U_{\text{tot}} = U_{\text{particles}} + U_B = \frac{aAL}{B^{3/2}} + \frac{VB^2}{8\pi} \tag{10.59}$$

The minimum of U_{tot} is reached for

$$B_{\text{min}} = \left(\frac{6\pi aAL}{V}\right)^{2/7} \tag{10.60}$$

while the equipartition B-field, for which $U_{\text{particles}} = U_B$ is

$$B_{\text{eq}} = \left(\frac{8\pi aAL}{V}\right)^{2/7} \tag{10.61}$$

Since the total energy for equipartition is $1.01U_{\text{min}}$, one often assumes synchrotron sources are in equipartition.

First noticed by Burbidge (1959).

Jets and IGM, IX

Radio lobes:

- Typical luminosity is a few times $L = 10^{44}\,\text{erg}\,\text{s}^{-1}$
- Typical B-fields are $\sim 10^{-4}\,\text{G}$

Assuming equipartition: typical energy content of a radio lobe: $E \sim 10^{60}\,\text{erg}$

corresponding to 10^7 supernovae

$\Longrightarrow$ lobe lifetime $t \sim E/L \sim 10^8\,\text{yr}$

$\Longrightarrow$ jets and lobes are rather long lived phenomena

Equipartition holds only approximately true for jets and lobes (see, e.g., Heinz & Begelman 1997).

Jet Formation, I

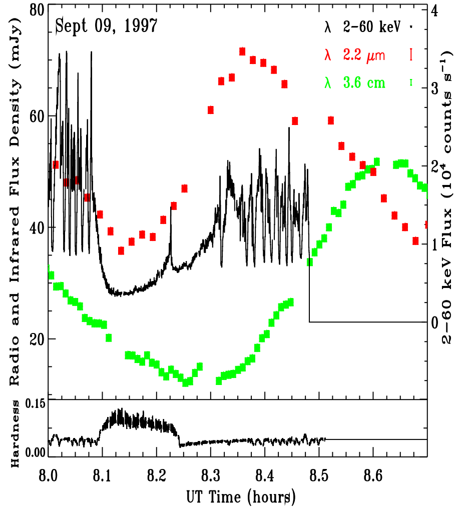

(GRS 1915+105; Mirabel et al., 1998)

Dynamics of jet formation are better studied in Galactic black holes with jets ("microquasars") because of shorter timescales.

Find clear X-ray–radio correlation (similar also seen in some AGN such as 3C120)

$\Longrightarrow$ "universal disk-jet-connection"

Jet Formation, II

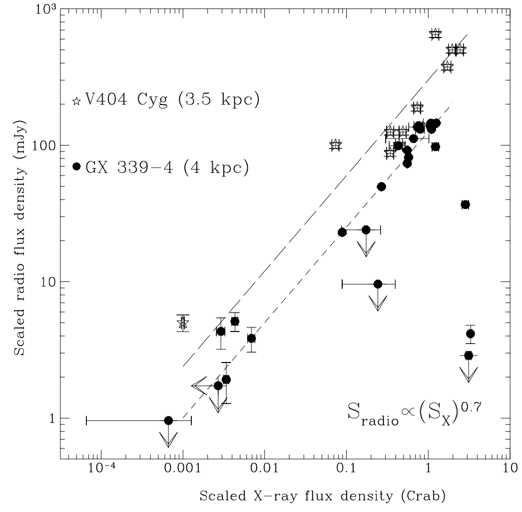

X-ray binaries: $S_{\text{radio}} \propto S_X^{0.7}$

$\Longrightarrow$ Radio and X-ray fluxes are correlated: evidence for interaction between disk and jet!

(Gallo, Fender & Pooley, 2003)

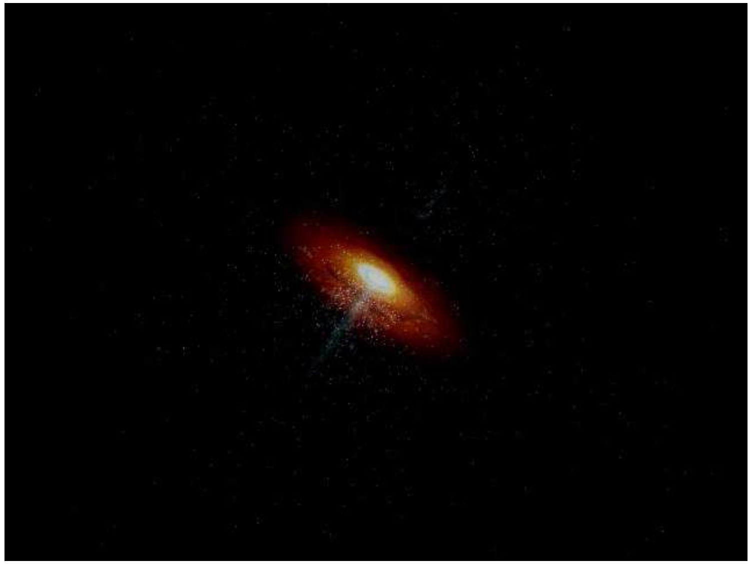

movie time: `jetmovies/agn_xray_020505_11_640x480_95pc`

Marscher et al. (2002): 3C120: X-ray dips followed by radio ejection events
$\Longrightarrow$ jets and accretion disk are related.

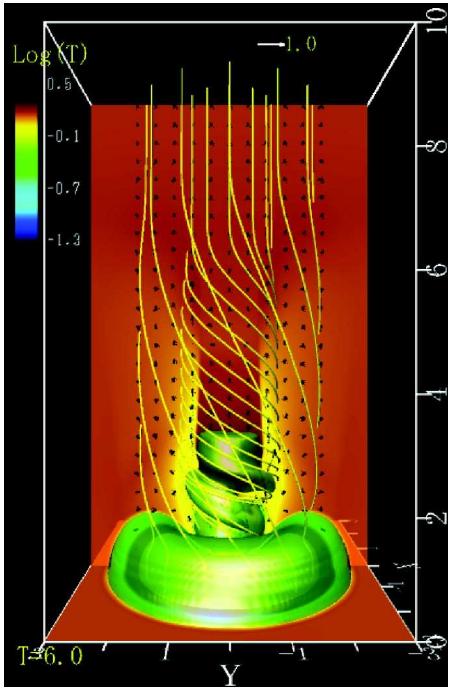

Temperature profile and B-field configuration of a MHD-jet

Movie: `jetmovies/d155mvj.avi`: Time evolution of B-field and density close to a BH (Matsumoto&Machida).

(Kigure & Shibata, 2005, Fig. 6)

Jet Formation, IV

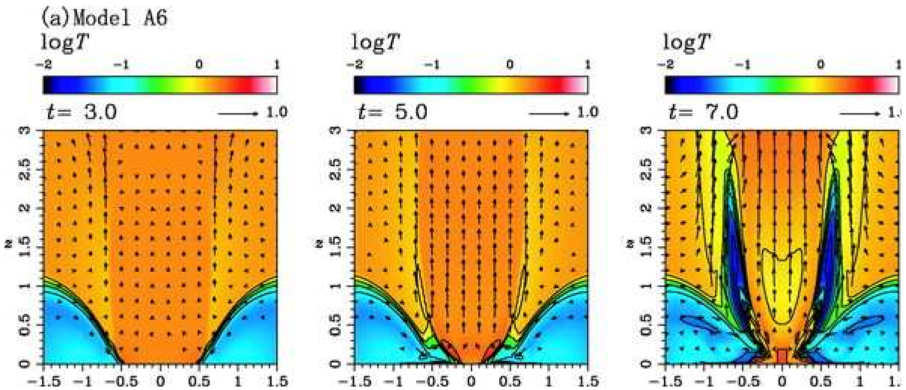

Evolution of a newly launched jet (Kigure & Shibata, 2005)

To study jet confinement and propagation: use magnetohydrodynamical simulations

Jet Formation, VI

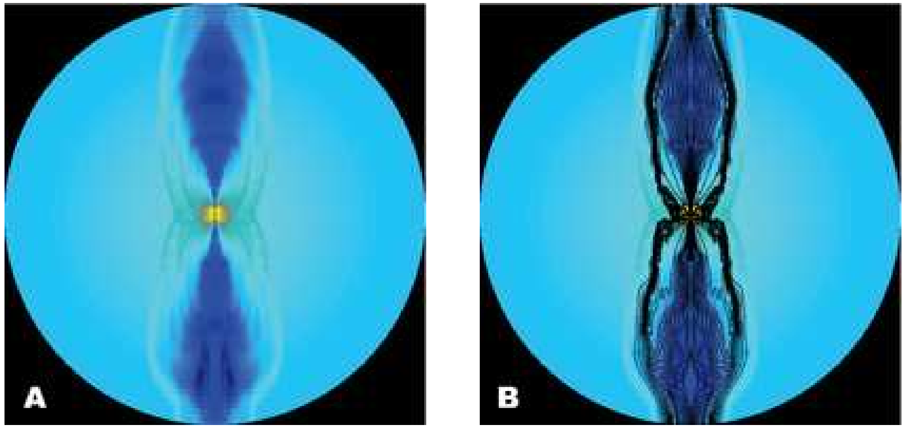

(McKinney, 2006, Fig. 1)

$\log\rho$ (left) and $\log\rho$ and B for a jet launched via a disk.

Outer radius is $10^4 GM/c^2$.

Jet Formation, VII

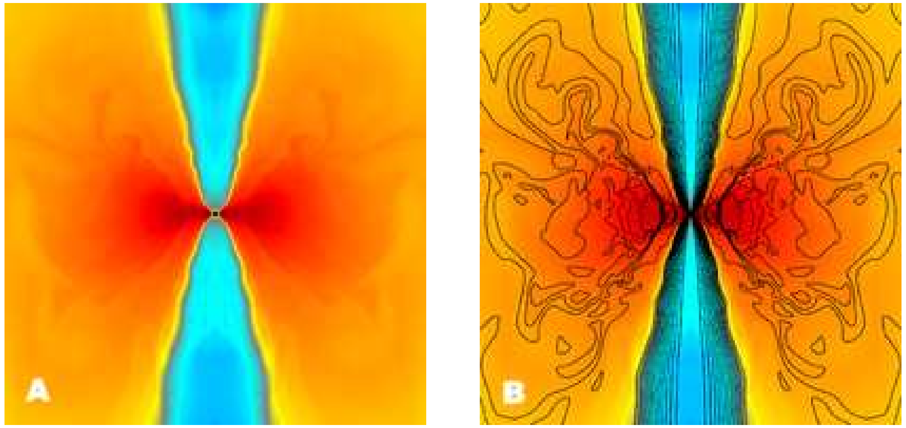

(McKinney, 2006, Fig. 2)

$\log\rho$ (left) and $\log\rho$ and B for a jet launched via a disk.

Outer radius is $10^2 GM/c^2$.

Aharonian, F., Akhperjanian, A. G., Bazer-Bachi, A. R., Beilicke, M., Benbow, W., & et al. 2006, Science, 314, 1424

Albert, J., et al., 2008, Astrophys. J., Lett., 685, L23

Biretta, J. A., Sparks, W. B., & Macchetto, F., 1999, ApJ, 520, 621

Burbidge, G. R., 1959, ApJ, 129, 849

Cheung, C. C., Harris, D. E., & Stawarz, Ł., 2007, Astrophys. J., Lett., 663, L65

Cohen, M. H., Cannon, W., Purcell, G. H., Shaffer, D. B., Broderick, J. J., Kellermann, K. I., & Jauncey, D. L., 1971, ApJ, 170, 207

Cohen, M. H., Lister, M. L., Homan, D. C., Kadler, M., Kellermann, K. I., Kovalev, Y. Y., & Vermeulen, R. C., 2007, ApJ, 658, 232

Condon, J. J., Cotton, W. D., Greisen, E. W., Yin, Q. F., Perley, R. A., Taylor, G. B., & Broderick, J. J., 1998, , 115, 1693

Conway, R. G., Garrington, S. T., Perley, R. A., & Biretta, J. A., 1993, A&A, 267, 347

Dermer, C. D., & Atoyan, A., 2004, Astrophys. J., Lett., 611, L9

Donato, D., Ghisellini, G., Tagliaferri, G., & Fossati, G., 2001, A&A, 375, 739

Fiorucci, M., Ciprini, S., & Tosti, G., 2004, A&A, 419, 25

Fossati, G., Maraschi, L., Celotti, A., Comastri, A., & Ghisellini, G., 1998, MNRAS, 299, 433

Gallo, E., Fender, R. P., & Pooley, G. G., 2003, MNRAS, 344, 60

Harris, D. E., Cheung, C. C., Biretta, J. A., Sparks, W. B., Junor, W., Perlman, E. S., & Wilson, A. S., 2006, ApJ, 640, 211

Harris, D. E., & Krawczynski, H., 2006, Ann. Rev. Astron. Astrophys., 44, 463

Heinz, S., & Begelman, M. C., 1997, ApJ, 490, 653

Kadler, M., Ros, E., Lobanov, A. P., Falcke, H., & Zensus, J. A., 2004, A&AS, 426, 481

Kadler, M., et al., 2008, ApJ, 680, 867

Kameno, S., Sawada-Satoh, S., Inoue, M., Shen, Z.-Q., & Wajima, K., 2001, PASJ, 53, 169

Kellermann, K. I., et al., 2004, ApJ, 609, 539

Kigure, H., & Shibata, K., 2005, ApJ, 634, 879

10–120

Jet Formation, VIII

Movie time:

- `diskmovies/rho3.mpg`: jet simulation out to $40GM/c^2$ (McKinney)
- `diskmovies/rout400new.lrho.3.mpg`: jet simulation out to $400GM/c^2$ (McKinney)

Killeen, N. E. B., Bicknell, G. V., & Ekers, R. D., 1986, ApJ, 302, 306

Kovalev, Y. Y., et al., 2005, AJ, 130, 2473

Kuehr, H., Witzel, A., Pauliny-Toth, I. I. K., & Nauber, U., 1981, , 45, 367

Laing, R. A., & Bridle, A. H., 1987, MNRAS, 228, 557

Lind, K. R., Payne, D. G., Meier, D. L., & Blandford, R. D., 1989, ApJ, 344, 89

Lister, M. L., et al., 2009, AJ, 137, 3718

Mannheim, K., 1993, A&A, 269, 67

Marscher, A. P., Jorstad, S. G., Gómez, J.-L., Aller, M. F., Teräsranta, H., Lister, M. L., & Stirling, A. M., 2002, Nature, 417, 625

Marshall, H. L., et al., 2001, Astrophys. J., Lett., 549, L167

Marshall, H. L., et al., 2005, ApJS, 156, 13

McKinney, J. C., 2006, MNRAS, 368, 1561

Mirabel, I. F., Dhawan, V., Chaty, S., Rodríguez, L. F., Martí, J., Robinson, C. R., Swank, J., & Geballe, T. R., 1998, A&A, 330, L9

Mizuta, A., Yamada, S., & Takabe, H., 2004, ApJ, 606, 804

Nilsson, K., Pursimo, T., Sillanpää, A., Takalo, L. O., & Lindfors, E., 2008, A&A, 487, L29

Perley, R. A., Bridle, A. H., & Willis, A. G., 1984, ApJS, 54, 291

Perlman, E. S., Biretta, J. A., Sparks, W. B., Macchetto, F. D., & Leahy, J. P., 2002, New Astronomy Review, 46, 399

Piner, B. G., Pant, N., & Edwards, P. G., 2008, ApJ, 678, 64

Pucella, G., et al., 2008, A&A, 491, L21

Raiteri, C. M., et al., 2001, A&A, 377, 396

Raiteri, C. M., et al., 2005, A&A, 438, 39

Raiteri, C. M., et al., 2006, A&A, 459, 731

Rybicki, G. B., & Lightman, A. P., 1979, Radiative Processes in Astrophysics, (New York: Wiley)

Sambruna, R. M., Gambill, J. K., Maraschi, L., Tavecchio, F., Cerutti, R., Cheung, C. C., Urry, C. M., & Chartas, G., 2004, ApJ, 608, 698

Shu, F. H., 1991, The Physics of Astrophysics, Vol. I. Radiation, (Mill Valley, CA: University Science Books)

Sikora, M., Begelman, M. C., & Rees, M. J., 1994, ApJ, 421, 153

Soldi, S., et al., 2008, A&A, 486, 411

Stawarz, Ł., & Ostrowski, M., 2002, ApJ, 578, 763

Tavecchio, F., Maraschi, L., & Ghisellini, G., 1998, ApJ, 509, 608

Tramacere, A., 2008, The Astronomer's Telegram, 1743, 1

Türler, M., et al., 2006, A&A, 451, L1

Türler, M., et al., 1999, A&AS, 134, 89

Whitney, A. R., et al., 1971, Science, 173, 225

Zensus, J. A., 1997, Ann. Rev. Astron. Astrophys., 35, 607